JOURNAL OF GEOPHYSICAL RESEARCH, VOL. 105, NO. B6, PAGES 13,755–13,777, JUNE 10, 2000

# Seismic wide-angle constraints on the crust of the southern Urals

R. Carbonell, [1] J. Gallart, [1] A. Pérez-Estaún, [1] J. Diaz,[1] S. Kashubin,[2] J. Mechie, [3] F. Wenzel, [4] and J. Knapp, [5]

**Abstract.** A wide-angle seismic reflection/refraction data set was acquired during spring 1995 across the southern Urals to characterize the lithosphere beneath this Paleozoic orogen. The wide-angle reflectivity features a strong frequency dependence. While the lower crustal reflectivity is in the range of 6-15 Hz, the *PmP* is characterized by frequencies below 6 Hz. After detailed frequency filtering, the seismic phases constrain a new average *P* wave velocity crustal model that consists of an upper layer of 5.0-6.0 km/s, which correlates with the surface geology; 5-7 km depths at which the velocities increase to 6.2-6.3 km/s; 10-30 km depths at which, on average, the crust is characterized by velocities of 6.6 km/s; and finally, the lower crust, from 30-35 km down to the Moho, which has velocities ranging from 6.8 to 7.4 km/s. Two different *S* wave velocity models, one for the N-S and one for the E-W, were derived from the analysis of the horizontal component recordings. Crustal sections of Poisson's ratio and anisotropy were calculated from the velocity models. The Poisson's ratio increases in the lower crust at both sides of the root zone. A localized 2-3% anisotropy zone is imaged within the lower crust beneath the terranes east of the root. This feature is supported by time differences in the *SmS* phase and by the particle motion diagrams, which reveal two polarized directions of motion. Velocities are higher in the central part of the orogen than for the Siberian and eastern plates. These seismic recordings support a 50-56 km crustal thickness beneath the central part of the orogen in contrast to Moho depths of ≈45 km documented at the edges of the transect. The lateral variation of the *PmP* phase in frequency content and in waveform can be taken as evidence of different genetic origins of the Moho in the southern Urals.

## 1. Introduction

The Ural mountains trend N-S and constitute the surface geographic and geological expression of part of the Uralide orogen, which formed the boundary between the former East European Craton (EEC) and Asia. It extends from the Aral sea in the south to Novaya Zemlya in the north. Because of the abundance of mineral and petroleum resources, this 3000-km-long orogenic belt has been a key target of extensive geological studies and geophysical experiments in the former Soviet Union. Geophysical exploration of the Urals started in the early 1940s. By that time the first seismicity map was compiled for the area *[Veis-Ksenofontova and Popov, 1940]*. Since then, more than 10,000 km of deep seismic sounding profiles had been acquired across the Urals at different latitudes *[Ryzhiy et al., 1992]*. While the first deep seismic data acquired suggested that the crustal thickness was on average 45 km *[Aleinikov et al., 1984]*, more recent geophysical data suggest an increase in crustal thickness beneath the orogen (up to 65 km) and the existence of a high-velocity most lower crustal layer (within the range of 7.7-8.0 km/s) *[e.g., Druzhinin et al., 1981, 1988; Egorkin and Mikhaltsev, 1990; Thouvenot et al., 1995; Berzin et al., 1996; Poupinet et al., 1997; Juhlin et al., 1997; Carbonell et al., 1998]*. The existence of this crustal root is particularly intriguing when the present low topographic relief and gravity field of the mountain belt are considered. Maximum elevations are offset from the root in the southern Urals conveying the idea that the present relief is unrelated to the root *[Berzin et al., 1996]*. The gravity data show a Bouguer minimum of about -40 to -50 mGal along the axis of the mountain belt *[Kruse and McNutt, 1988; Döring et al., 1997]*, pointing to the existence of an anomalously dense crust. On the other hand, apatite fissiontrack ages show that the Urals have remained relatively stable since early Mesozoic times *[Seward et al., 1997]*. The preservation of a crustal root beneath the Uralide orogen is an anomalous feature when compared with orogens of similar age. For example, the

[1]Department of Geophysics, Institut de Ciències de la Terra "Jaume Almera" Consejo Superior de Investigaciones Científicas, Barcelona, Spain

[2]Bazhenov Geophysical Expedition, Scheelite, Russia

[3]GeoForschungsZentrum, Potsdam, Germany

[4]Geophysical Institute, Karlsruhe University, Karlsruhe, Germany

[5]Institute for the Study of the Continents, Cornell University, Ithaca, New York



Paper number 2000JB900048.
0148-0227/00/2000JB900048$09.00

Caledonides *[Matthews and Cheadle, 1986]*, the Variscides *[Meissner and Wever, 1986; Matte and Hirn, 1988]*, and the Appalachians *[McBride and Nelson, 1991]* all lack a crustal root. However, the recent identification of a root beneath the Proterozoic Trans-Hudsonian orogen *[Lucas et al., 1993]*, together with the Uralide root raise important questions concerning the formation and preservation of crustal roots and orogen evolution.

The wide-angle seismic data presented here is part of a multi-seismic experiment acquired across the southern Urals in 1995 (URSEIS'95) *[e.g., Berzin et al., 1996]* within the EUROPROBE programme *[Gee and Zeyen, 1997]*. The URSEIS'95 consisted of a combined multi-seismic exploration *[Carbonell et al., 1996; Echtler et al., 1996; Knapp et al., 1996]* of the southern Uralide orogen from Sterlitamak in the west to the Kazakhstan border in the east.

In a preliminary interpretation of the wide-angle data, *Carbonell et al., [1996]* estimated a crustal velocity model constrained by shot gathers 1 and 4. Neither middle nor lower crustal arrivals were identified in these shot gathers. The model was characterized by a lack of information in the core of the orogen because of the low quality of shot records 2 and 3. *Carbonell et al., [1998]* imaged the Moho beneath the root zone by performing a stack of the wide-angle data. In the present study we discuss the frequency dependence of the seismic phases; we increase the quality of the data set by careful frequency filtering revealing middle and lower crustal events; we determine a new and better constrained $P$ wave velocity model including shot records 2 and 3; we analyze and interpret the horizontal component of the wide-angle data constraining a $S$ wave velocity model; and, finally, we discuss some of the geological implications of these models and determine the seismic differences between the crustal domains that build up the orogen.

## 2. Geologic and Geophysical Framework

The Uralian crustal structures are thought to have developed from collisional accretion of volcanic arc and microcontinental fragments with the former east European continental margin *[Hamilton, 1970; Zonenshain et al., 1984, 1990; Puchkov, 1997; Brown et al., 1997]* from Late Devonian through the Permian and into the Triassic *[Ivanov et al., 1975; Ivanov and Rusin, 1986; Khain, 1985; Zonenshain et al., 1984, 1990; Brown et al., 1996]*. The Main Uralian Fault (MUF), which separates the EEC from the accreted terranes to the east of the Urals, along the arc-continent suture zone, is a wide, east dipping serpentinitic melange zone (Figure 1). The footwall to the MUF in the southern Urals consists of a west vergent thrust stack of Archean through Paleozoic rocks, structurally overlain by several allochthonous units *[Brown et al., 1996, 1997; Pérez-Estaún et al., 1997]*.

To the east of the suture zone are the Upper Silurian to Upper Devonian volcanics and volcaniclastics and the Carboniferous sediments of the Magnitogorsk volcanic arc, which are folded into an open synform *[Seravkin et al., 1992; Ivanov and Ivanov, 1991; Sokolov, 1992]*. To the east, highly metamorphosed rocks of continental nature with structures verging toward the east, form the east Uralian Zone *[Echtler et al., 1996; Puchkov, 1997]*. Farther east, Precambrian rocks are overlain by Ordovician and Carboniferous sediments and in places have been overthrust by Ordovician to Devonian ophiolite suites and volcanic and volcaniclastic rocks of island arc affinity *[Ivanov and Ivanov, 1991]*. All units to the east of the MUF were intruded by granitic rocks during the late Devonian to Permian times *[Fershtater et al., 1997]*. Mesozoic-Cenozoic sediments of the west Siberian basin cover large regions of the Trans-Uralian Zone.

Descriptions of the crustal structure beneath the Uralide orogen, based on different geophysical datasets, are given by *Kruse and McNutt [1988], Avtoneyev et al., [1992], Sokolov [1992] and Ryzhiy et al., [1992]*, among others. UWARS *[Thouvenot et al., 1995; Poupinet et al., 1997]*, ESRU *[Juhlin et al., 1995, 1997]* and URSEIS *[Echtler et al., 1996; Knapp et al., 1996; Carbonell et al., 1996; Steer et al., 1998]* experiments present seismic transects across the Urals at different latitudes. UWARS and ESRU experiments were carried out north of Ekaterinburg in the central Urals and revealed a moderate increase in the crustal thickness of 3-5 km. URSEIS'95 near vertical, common midpoint CMP coincident explosion and vibroseis images show that the crustal reflectivity varies laterally and can be correlated with major tectonic units and different terranes, suggesting that the internal structure of the southern Urals is that of a preserved (since Paleozoic times) bivergent collisional orogen *[Echtler et al., 1996; Knapp et al., 1996]*. The reflective Moho is well defined in the eastern and westernmost part of the URSEIS'95 explosion profile deepening into the central part of it but does not appear as a distinctive feature in this central part *[Steer et al., 1998]*.

## 3. Data Description and Processing

A total of 33,000 kg of explosives distributed among 15 shots, with charge sizes that ranged between 1500 and 3000 kg (Figures 1 and 2) were used in this survey. The seismic energy was recorded by 50 three-component digital recording instruments (REFTEK and Lennartz) in successive deployments. The difficult logistics forced station spacings that range from 1 to 2.5 km. Spatial aliasing due to the large trace spacing prevents a good lateral resolution of the internal structure of the reflecting bodies. The origin times were recorded by a digital recording seismograph installed at the source location. Further details on the acquisition are given by *Carbonell et al.,[1996]*. The main transect consisted of four shot records at 120-km intervals (Figure 2). The explosion shots generated reversed recordings with offset coverage from 0 to 340 km.

Shot gathers were assembled for all vertical and horizontal components for a total time of 120 s at a sample rate of 0.008 s and stored in SEGY format. The processing included editing of bad traces, attenuation of noise, trace scaling, and frequency filtering. In order to account for source and receiver coupling differences the traces were balanced by the

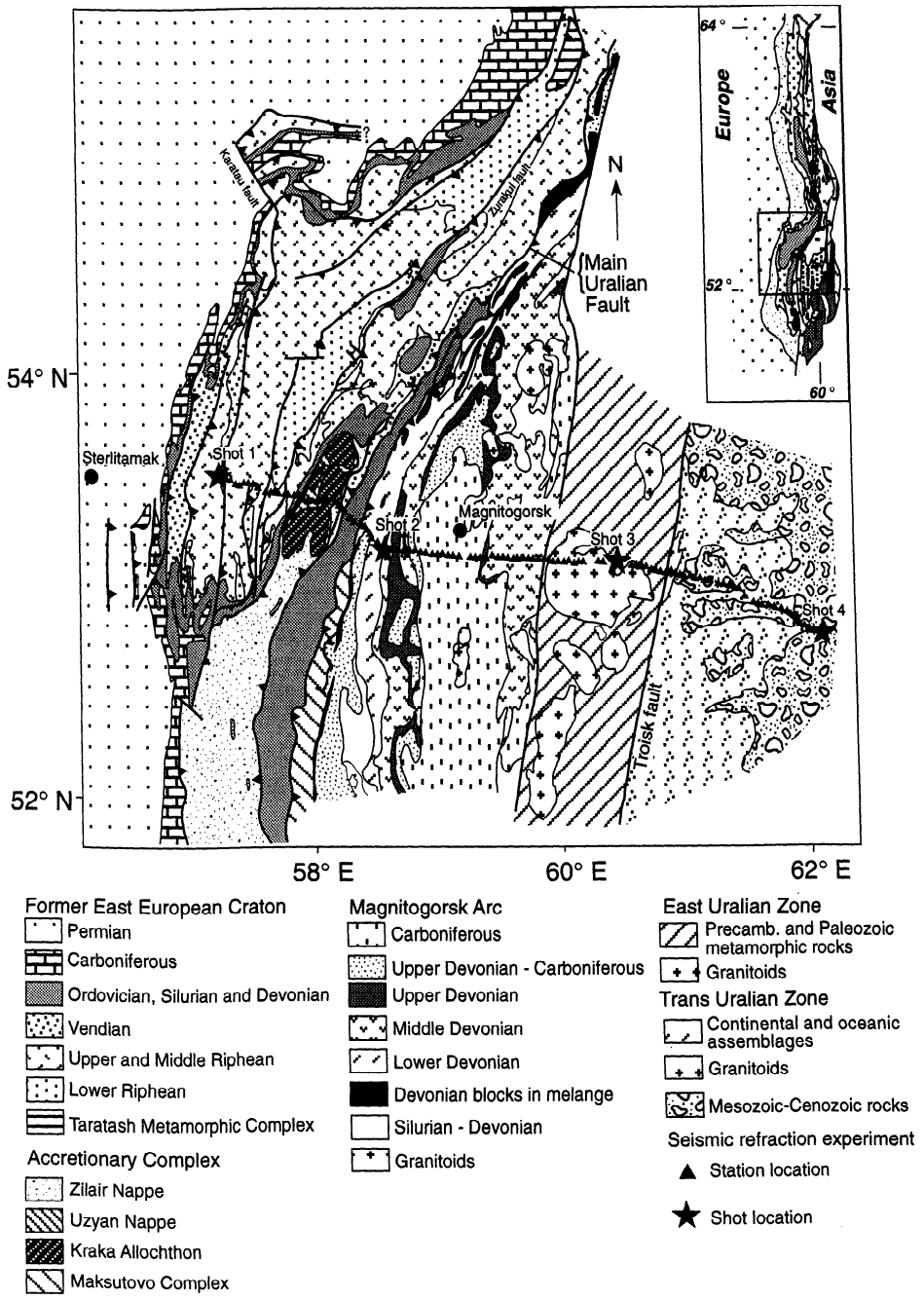


**Figure 1.** Location of the URSEIS'95 deep seismic experiment. Geologic sketch map indicates the major geologic units and tectonic structures of the southern Urals. Inset map shows the location of the study area in the southern Urals. The experiment design with the station distribution (inverted triangles) and shot point locations (stars) are also marked.

root mean square (RMS) of the background noise, and the amplitudes of the last second of the data were used to estimate the background noise *[Carbonell et al., 1998]*.

The preliminary interpretation of the URSEIS'95 wide-angle data *[Carbonell et al., 1996]* could not constrain in detail the velocity-depth features beneath the central part of the studied area due to the limited resolution of the wide-angle arrivals from shot points 2 and 3. Therefore we have tried to enhance the signature of these phases in the processing stage by analyzing their frequency content. Using a filter panels technique *[Sheriff and Geldart, 1982; Yilmaz, 1987]* we found that they exhibit a narrow band of dominant frequencies which differ from phase to phase and from shot to shot. Although frequencies up to 15 Hz are recorded, the spectra of lower crustal and Moho reflections are dominated by low frequencies (Figure 3), especially from shots 2 and 3, in the range of 2 to 7 Hz.This frequency dependence has been identified in all three components. Hence we have per-

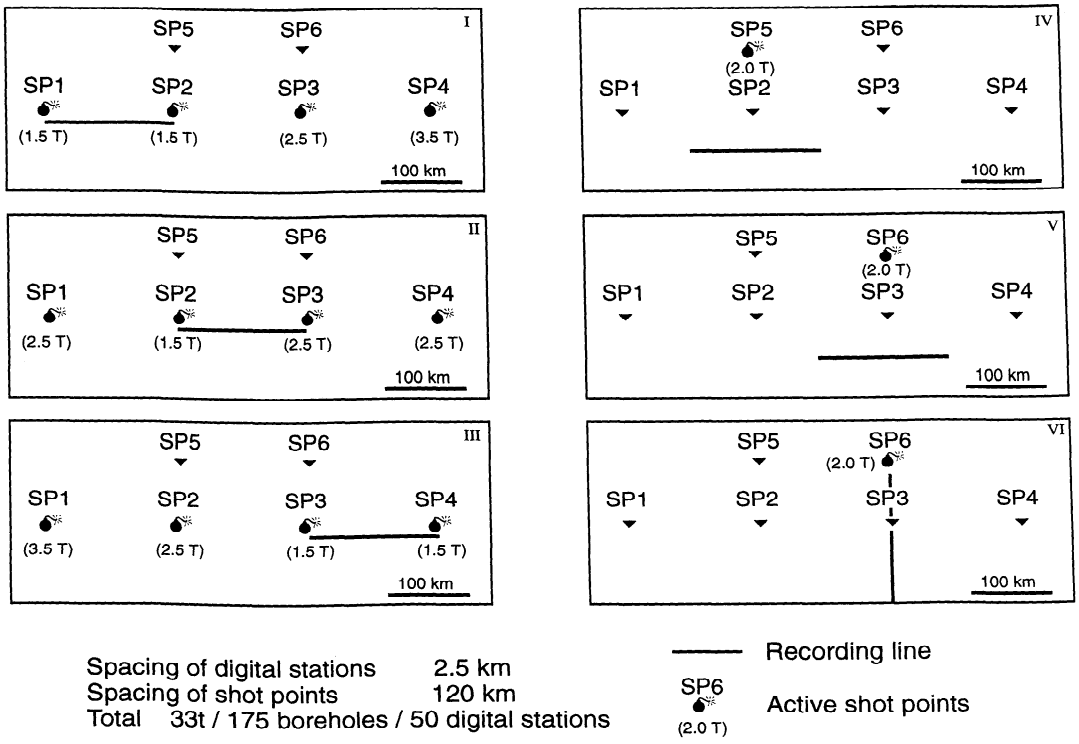


**Figure 2.** Design of the seismic wide-angle/refraction data acquisition experiment indicating the location of the recording instruments (recording line) and the shot points with the approximate charge sizes.

formed a new, more accurate interpretation of the wide-angle data in southern Urals using the travel time picks obtained after iterative filtering to best resolve each seismic phase.

For the frequency band up to 15 Hz some seismic events appear as bursts of energy where the waveform does not correlate from trace to trace (for example the *PmP* phase in shot records 3 and 4 in Figure 4 and shot record 2 in Figure 5). With this frequency band the uncertainty of phase picking is unreasonably large. Therefore any velocity model derived from these travel time picks has to be considered as poorly constrained. A low pass filter up to 6 Hz reveals a sharp *PmP* arrival and the waveform can then be followed from trace to trace (Figures 4 and 5). Figure 5 also illustrates the frequency dependence of the seismic events for shot record 2. Event *LC* is a relatively high-frequency phase traced within 75-200 km offset that precedes the *PmP*. Event *LC* can be associated with the top of the lower crust, and it is attenuated when the data are high cut at 4.5 Hz. This event had not been indentified in previous interpretations of the data *[Carbonell et al., 1996, 1998]*. However, this low pass filter emphasizes the *PmP* arrival for the offset range of 80-250 km. These differences in the frequency characteristics of the seismic events are probably a result of the geologic fabric or structure.

The *Pg* arrivals are characterized by a sharp increase in amplitude of the trace and by frequencies above 6 Hz (Figures 4 and 5). The *PmP* is also identified by its high amplitude, but it is better resolved for frequencies below 6 Hz (Figures 4 and 5). The *Pn* upper mantle refracted phase (shot record 4, Figure 4) is a high-frequency first arrival for offsets larger than 250 km in contrast with the low frequency that characterizes the *PmP* phase.

The effect of the low pass filtering is more dramatic on the horizontal components (Figures 6 and 7). The shot gathers with a frequency band up to 15 Hz do not display laterally coherent events. The events can be correlated laterally when the data are low cut at 8 Hz and when the data are further low cut at 4.5 Hz (Figures 6 and 7). In some cases, the characteristics of the event change laterally. When a 4.5 Hz high cut filter is applied to the data, an event preceding the *SmS* can be identified. This frequency band attenuates the first shear wave arrivals while it emphasizes deeper events, especially the *SmS* phase (Figure 7). The N-S and E-W horizontal components display prominent differences. Usually, events are better identified in the N-S than in the E-W horizontal component; see, for example, the *LC* event in shot record 3 (Figures 7, 8 and 9) and the upper crustal event in shot record 2 (Figure 8). The N-S and E-W horizontal components also show differences in the arrival time of the *SmS* phase (at offsets of 175-300 for shot records 2 and 4, Figures 8 and 9).

The good quality of the data for all the components after low pass filtering makes it possible to determine one *P* wave velocity model and two *S* wave velocity models (one for the N-S component and a second for the E-W component). The velocity model achieved by travel time fitting using ray-tracing techniques was further refined by amplitude modeling *[Zelt and Smith, 1992]*. The fitting between

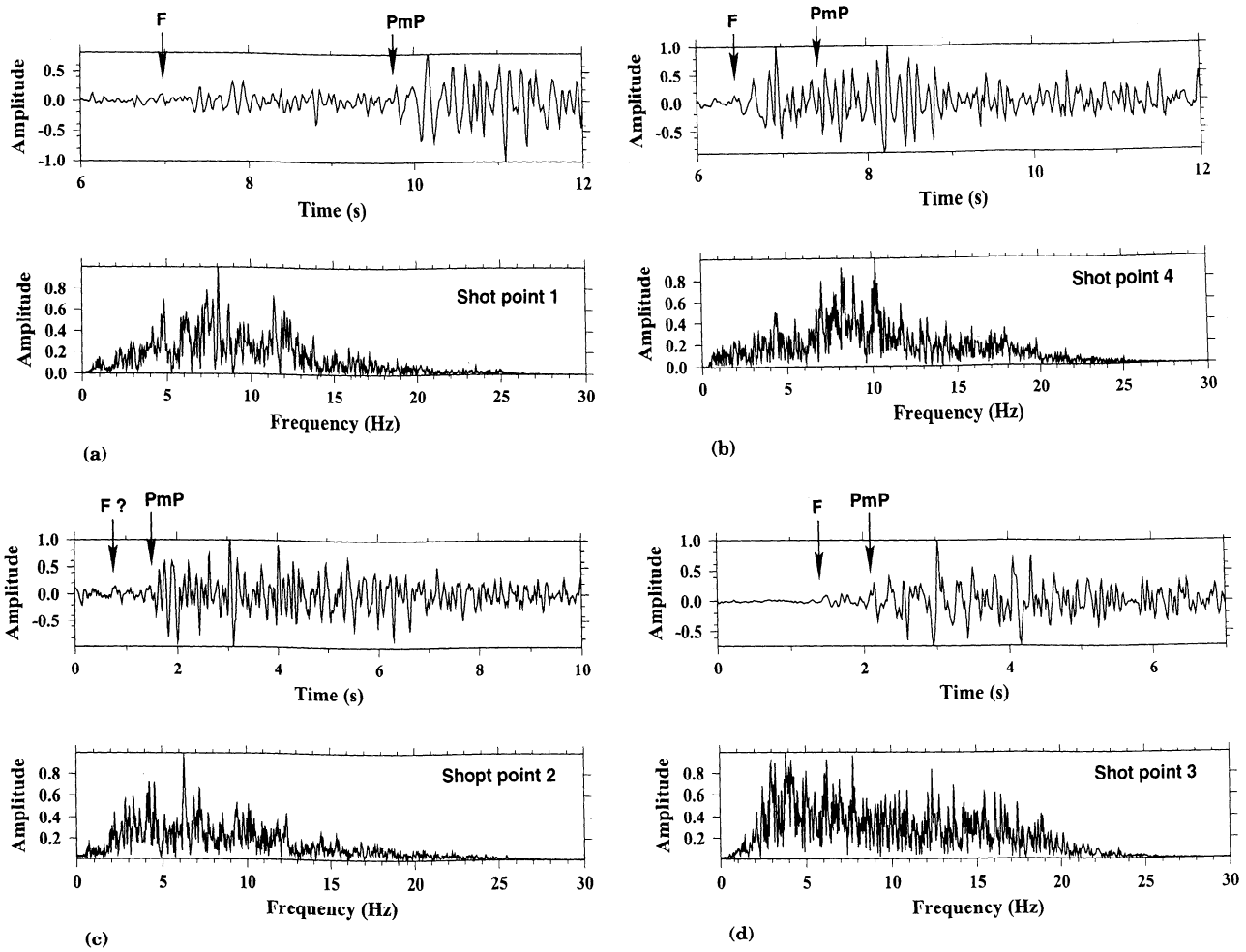


**Figure 3.** Averaged spectra for shot gathers 1 to 4 for selected offset ranges (to calculate the average spectra the traces within the specified offset range were stacked). (a) Stacked trace and average frequenc y spectra for shot gather 1. To obtain this spectra, we stacked the traces within offsets 155-161 km (three traces). (b) Same as Figure 3a, except for shot point 4 for the offset range of 179-185 km (four traces). (c) Same as Figure 3a, except for shot point 2 for the offset range of 208-214 km (four traces). (d) Same as Figure 3a, except for shot point 3 for the offset range of 198-204 km (three traces). The average spectra were calculated from the stacked trace and normalized. Before stacking, the traces were balanced by the RMS of the noise (see text for explanation). F indicates the first arrivals and the *PmP* indicates the starting time of the *PmP* onset.

the predicted theoretical travel time arrivals and the observed phases for the vertical component is shown in Figure 10. In order to better correlate the crustal phases, shot gathers were reduced by velocities of 6 km/s for the vertical components. To resolve upper mantle arrivals, a velocity reduction of 8 was used in some cases. In S record sections a $\sqrt{3}$ factor was used in the travel timescale and in the reduction velocities with respect to the corresponding P record sections, in order to evaluate deviations of the Poisson's ratio from the average value of 0.25, since for this value the analogous P and S phases should coincide when P and S record sections are overlain. Thus new insight on the crustal composition of the crust beneath the southern Urals is gained by comparing the correlations between the vertical and the horizontal components. With the $V_p$ and $V_s$ velocity models we can estimate $V_p/V_s$ or alternatively the distribution of the Poisson's ratio within the crust using:

$$\sigma = \frac{(\frac{\alpha}{\beta})^2 - 2}{2[(\frac{\alpha}{\beta})^2 - 1]}, \quad (1)$$

where $\alpha$ and $\beta$ denote the $P$ and $S$ wave velocities. Additionally, owing to the qualitative and quantitative differences between the N-S and E-W record sections two different $S$ wave velocity models ($V_s^{NS}$, $V_s^{EW}$) can be determined. Then $\beta$ in (1) will be the average velocity $(\beta_{NS} + \beta_{EW})/2$. The comparison between $Vs^{NS}$ and $Vs^{EW}$ suggests the existence of velocity differences between polarized shear waves, which is an indication of anisotropic features in the crust. The distribution of the percent of anisotropy ($a$) within the crust can

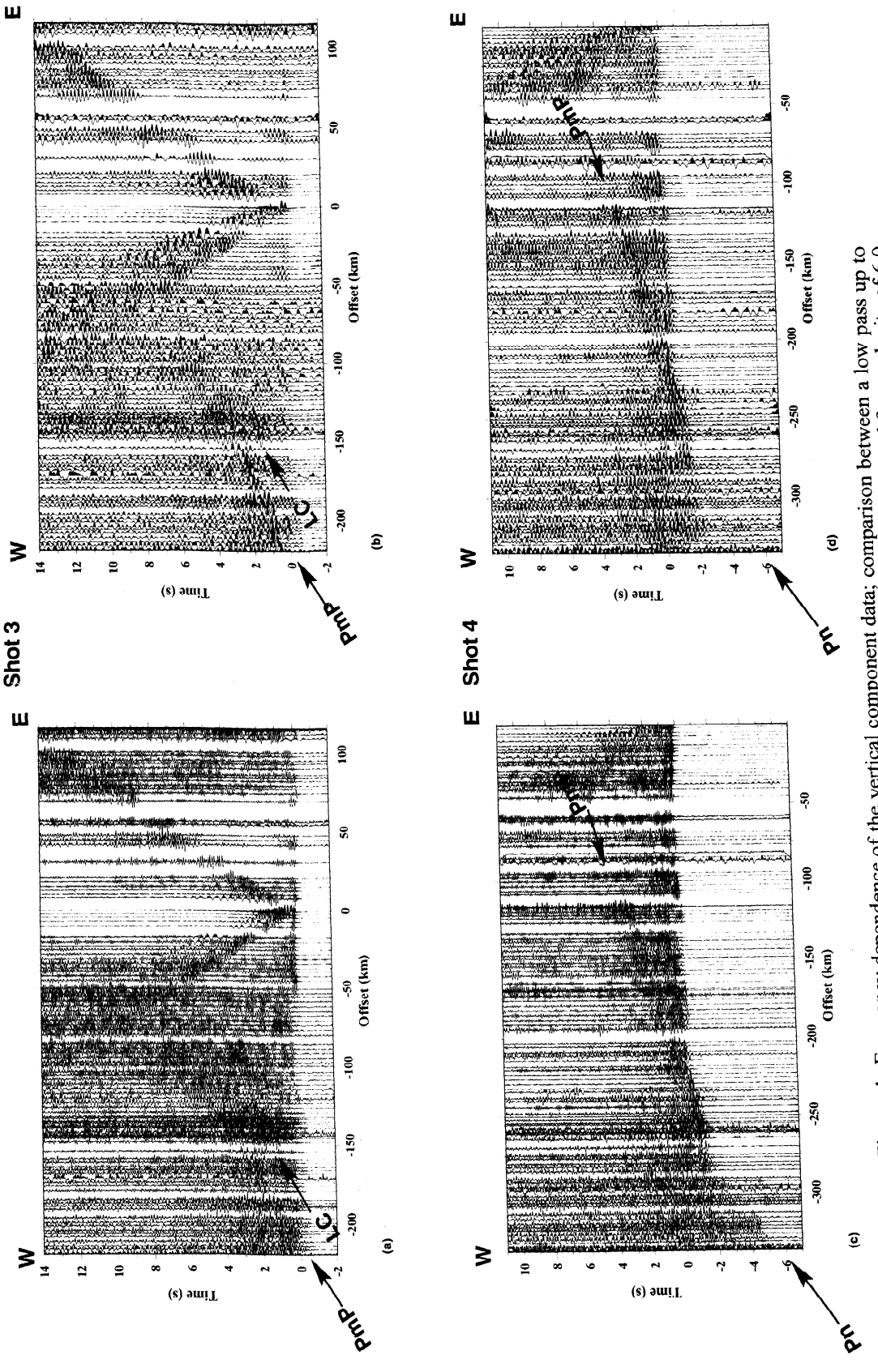


**Figure 4.** Frequency dependence of the vertical component data; comparison between a low pass up to 15 Hz and a low pass up to 6 Hz for two shot records. The data have been reduced for a velocity of 6.0 km/s. (a) Shot record 3 low passed up to 15 Hz. (b) Shot record 3 low passed up to 6 Hz. (c) Shot record 4 low passed up to 15 Hz. (d) Shot record 4 low passed up to 6 Hz. Low pass filtering increases the lateral correlation of the *PmP* phases resulting in a better resolved image. *PmP* marks the *P* wave reflected from the Moho. *LC* marks the arrivals from the lower crust; *Pn* is the refracted wave from the upper mantle.

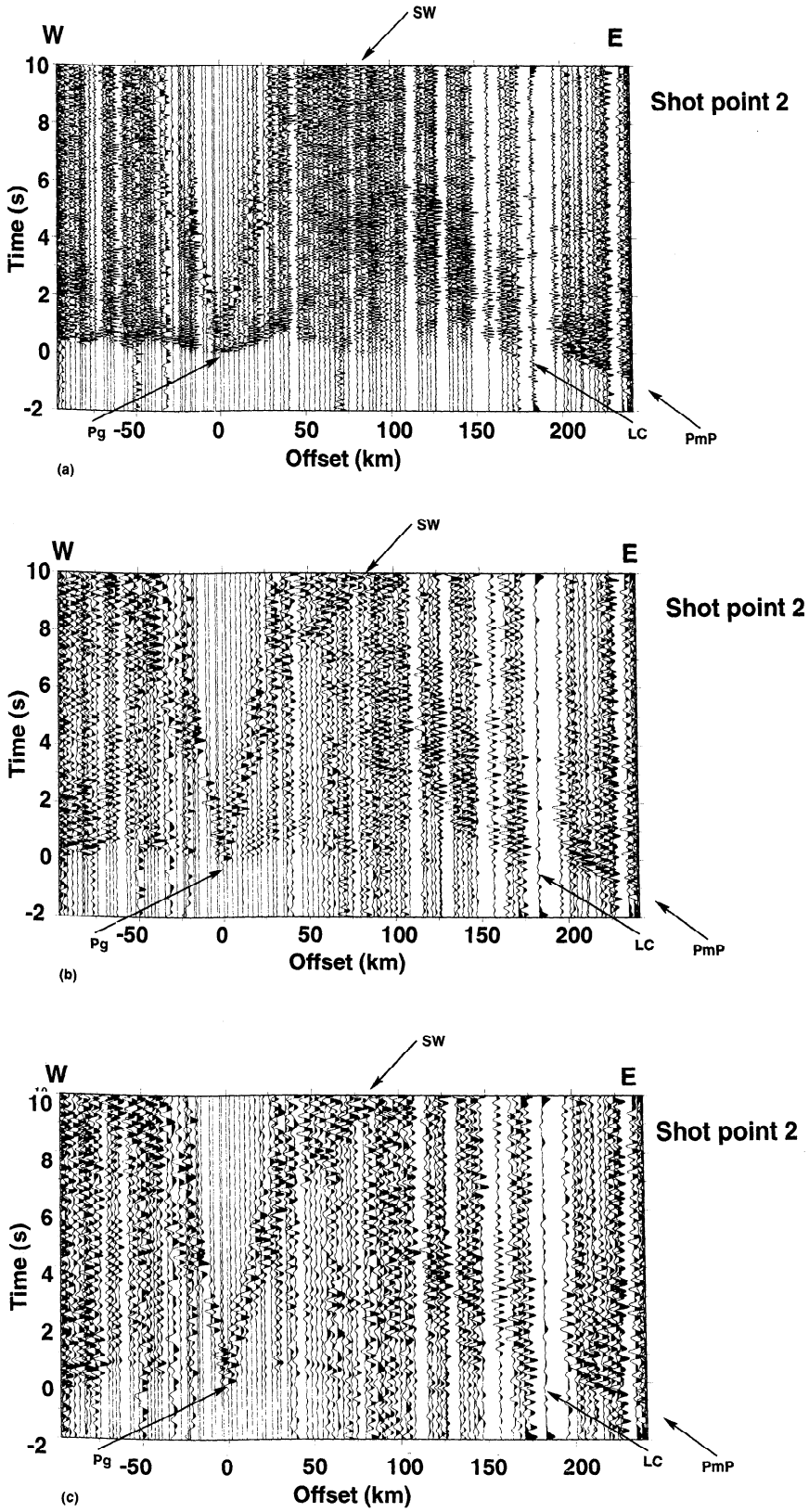


**Figure 5.** Frequency dependence of the lower crustal reflectivity; comparison between (a) low pass filtered data up to 15 Hz, (b) a low pass filter up to 6 Hz, and (c) a low pass filter up to 4 Hz (c) for the vertical component of shot 2. Notice the sharp increase in reflectivity for the *LC* in Figures 5a and 5b, whereas it is attenuated in Figure 5c. The data are plotted with a velocity reduction of 6.0 km/s. *Pg* indicates the first arrival, which is also characterized by high frequencies; it is strongly attenuated in Figures 5b and 5c.

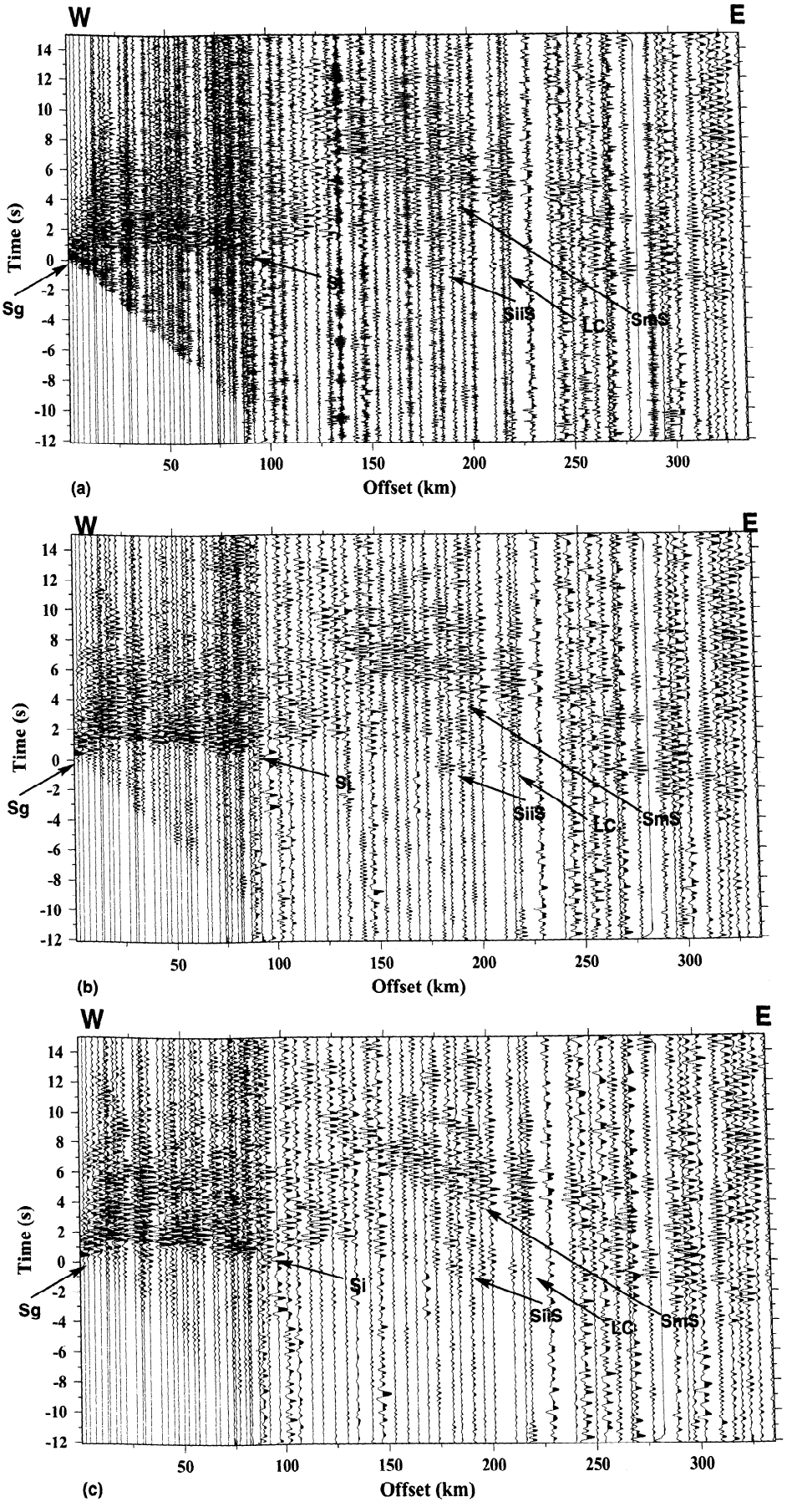


**Figure 6.** Comparison for the N-S horizontal component of shot gather 1 low pass filtered up to: (a) 15 Hz, (b) 6 Hz, and (c) 4.5 Hz. *Sg* denotes the direct arrival, *Si* and *SiiS* denote the two upper crustal events, *LC* denote a lower crustal event, and *SmS* denotes the *S* wave reflected at the Moho. The data are plotted with a velocity reduction of 3.46 km/s. Note the improvement in the signal after low pass filtering. In particular, the *LC* event prior to *SmS* is identified only after low pass fitering in Figure 6b.

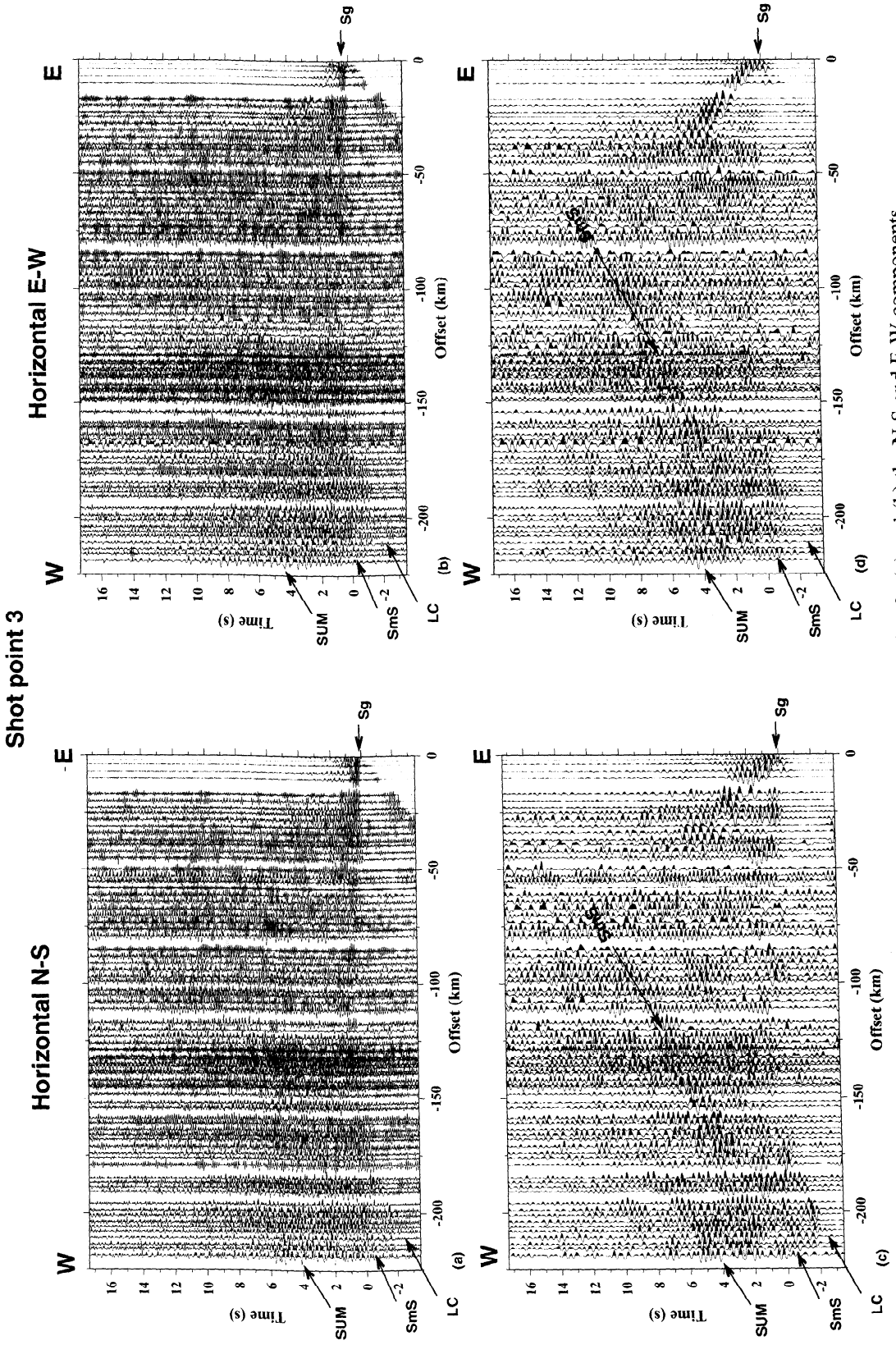


**Figure 7.** N-S and E-W horizontal records for shot gather 3. (a) and (b) the N-S and E-W components low pass filtered up to 15 Hz, respectively. (c) and (d) N-S and E-W component low pass filtered up to 4.5 Hz, respectively. The data are plotted with a velocity reduction of 3.46 km/s. *SmS* marks the shear wave reflected at the Moho, *LC* makrs a lower crustal phase and *Sg* marks the first *S* wave arrival, which is characterized by high frequencies. The *Sg* phase is very sharp in Figures 7a and 7c, and it has been attenuated by the low pass filter in Figures 7b and 7d. *LC* is better identified in the N-S component after low pass filtering (Figure 7b), and it is almost missing in Figure 7d. SUM indicates a burst of energy probably reflected in the upper mantle, and it is imaged in the N-S component.

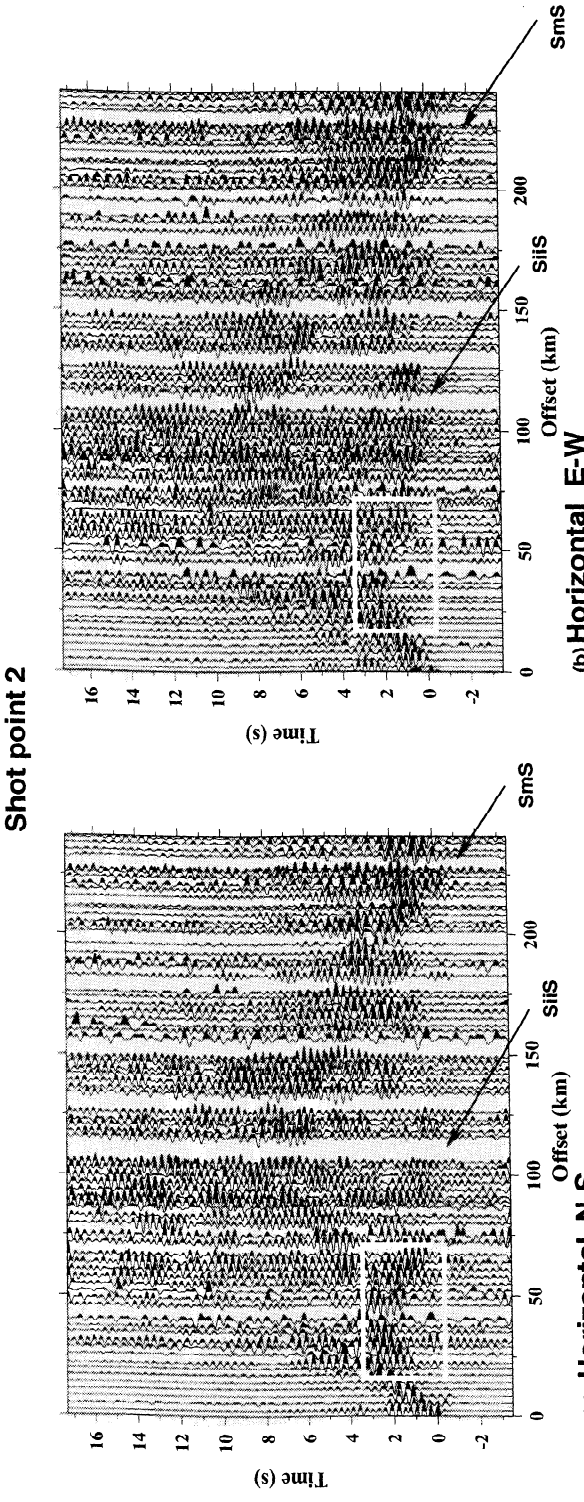


**Figure 8.** N-S (a) and E-W (b) horizontal components of shot record 2 low pass filtered up 4.5 Hz. The data are plotted with a velocity reduction of 3.46 km/s. The box between 0 and 75 km offset highlights the delay of the first arrivals (*Sg*) which is presumably due to the Carboniferous metasediments in the Magnitogorsk volcanic arc (in violet in Plate 1). *SiiS* and *SmS* mark energy reflected in the upper, lower crust, and Moho levels. The white line close to *SmS* indicates the predicted travel time ($t_{SmS(0.25)}$) for the *SmS* using the *S* wave velocity model derived from the *P* wave velocity model assuming a $\sigma$ (Poisson's ratio) of 0.25. The interpreted *SmS* is delayed with respect to the $t_{SmS(0.25)}$ for both components which suggests deviations in $\sigma$ from 0.25. Note also the difference in the location of the interpreted *SmS* in both components. The *SmS* for the N-S component Figure 8a is delayed with respect the *SmS* of the E-W component Figure 8b. These travel time differences suggest the existence of two different velocities for the *S* wave energy and therefore of anisotropy.

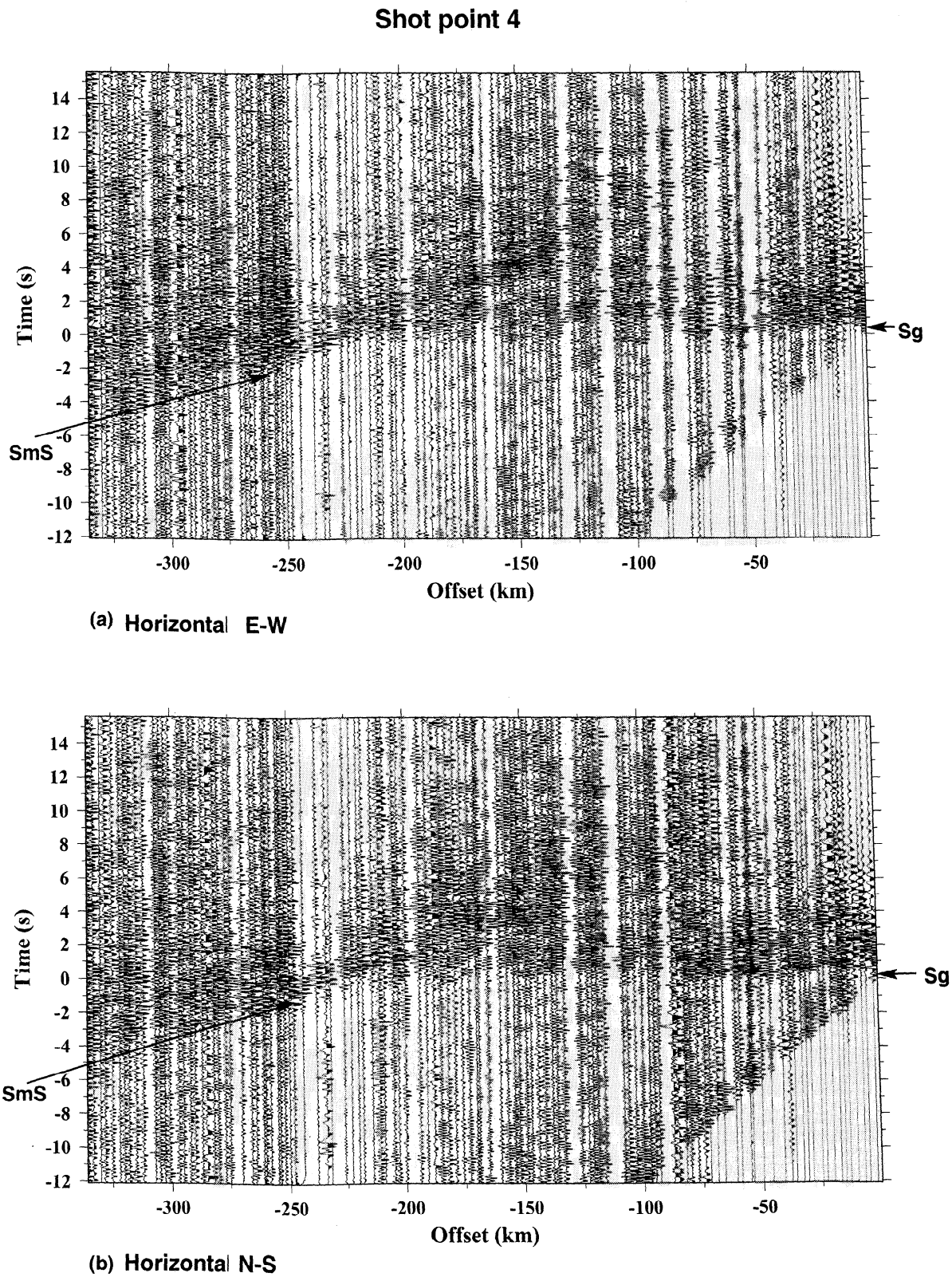


**Figure 9.** (a) E-W and (b) N-S horizontal components of shot gather 4 low pass filtered up to 8 Hz. *Sg* indicates the first arrival, and the *SmS* indicates the *S* wave energy reflected at the Moho. The data are plotted with a velocity reduction of 3.46 km/s. The *SmS* travel times ($t_{SmS(0.25)}$) predicted by an *S* wave velocity model derived from the *P* wave velocity model assuming a Poisson's ratio ($\sigma$) of 0.25 is indicated by the white line. The interpreted *SmS* is delayed with respect to the $t_{SmS(0.25)}$ for both components which suggests deviations in $\sigma$ from 0.25. Additionally, the arrival times of the *SmS* in the E-W component are delayed with respect to those observed in the N-S. These differences support the existance of two different velocities for the *S* wave energy (anisotropy) as in Figure 8.

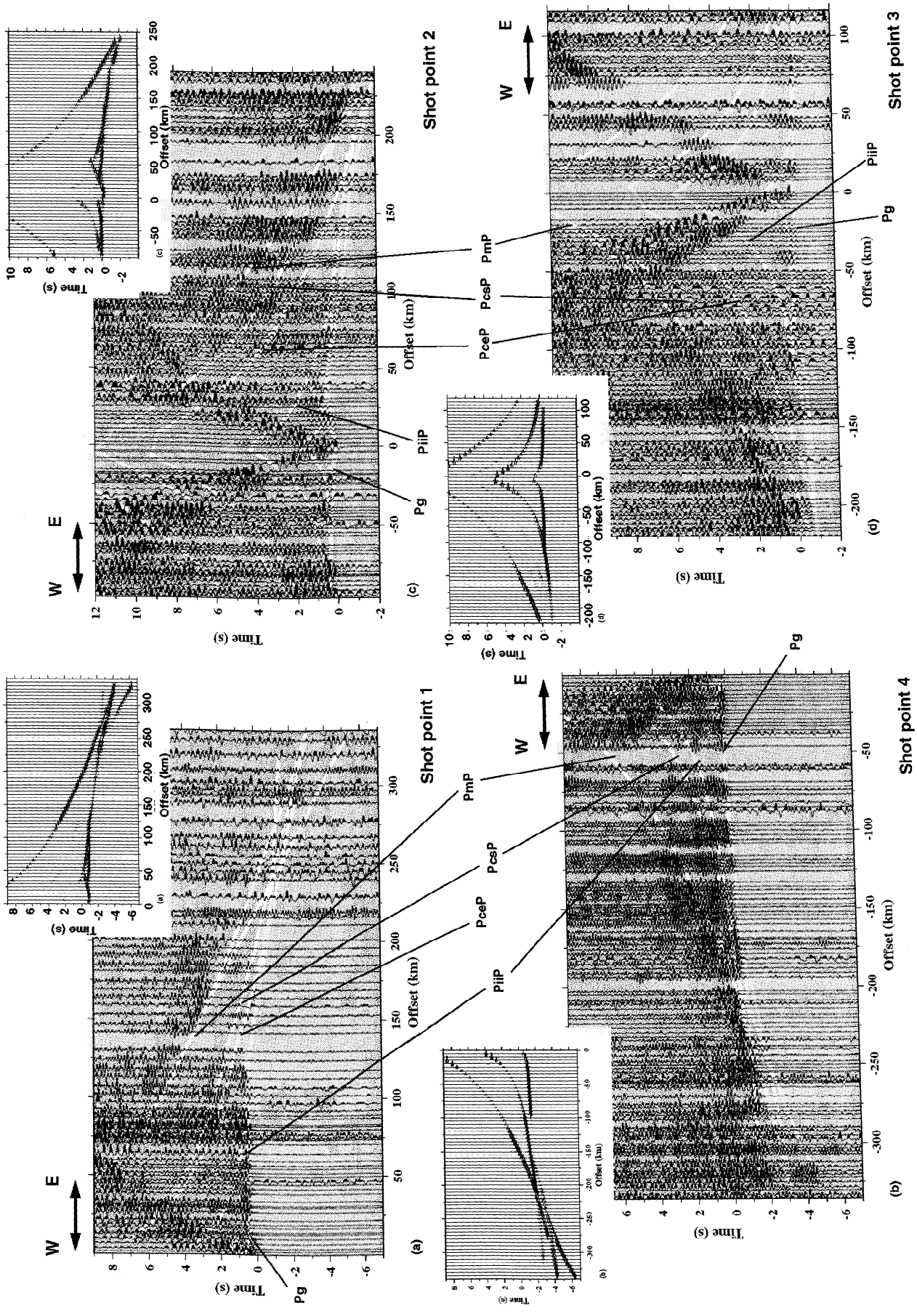
Shot point 1
Shot point 2
Shot point 3
Shot point 4
W
E
Pg
PmP
PcsP
PceP
PiiP
Time (s)
Offset (km)
(a)
(b)
(c)
(d)

be estimated using:

$$a = 100\left(\frac{|\beta_{NS} - \beta_{EW}|}{\frac{\beta_{NS}+\beta_{EW}}{2}}\right), \quad (2)$$

where $\beta_{NS}$ and $\beta_{EW}$ correspond to the $S$ wave velocities derived from the N-S and E-W oriented horizontal component record section, respectively. It is very important to bear in mind that although the data set is characterized by well-resolved arrivals, only the large-scale features of the images obtained using (1) and (2) are physically meaningful.

## 4. Crustal Features

### 4.1. *P* Wave Data

The vertical component record sections of the four shot records along the E-W main transect are characterized, after appropriate filtering, by a number of prominent seismic phases that can be correlated in each shot gather and are identified accordingly in the others. All phases have been labeled following conventional criteria as *Pg*, *Pn* for refractions within the shallow crust and upper mantle, respectively, and *PiiP*, *PcP*, and *PmP* for reflections in the middle crust, lower crust, and the Moho, respectively. The frequency filtering and careful modeling suggested that the *PcP* phase beneath the Magnitogorsk volcanic arc could be interpreted as two events labeled in this study as *PcsP* and *PceP*.

In shot record 1 (Figure 10), up to 20 km offset, first arrivals show an apparent velocity of 5.2 km/s, increasing beyond that to 6.0 km/s. This *Pg* phase is a rather homogeneous, high-amplitude wave train that can be identified up to 120 km offset. In the other three shot gathers the *Pg* is observed almost from the source location at reduced times about zero (where the basement outcrops) up to similar distances. This event is especially prominent in the high-frequency plots (Figures 4 and 5). In all shot records, at ≈100 km offset the high amplitudes of the first arrivals reveal a constructive interference of the *Pg* wave train with a reflected phase in the upper crust, around 6-7 km depth, where the velocity increases to 6.2 km/s. The most significant anomaly in the *Pg* phase is found toward the east of shot record 2, where arrivals at 20-60 km offset are progressively delayed, with a shift of 0.5 s centered at 40 km offset (Figure 5). Such a delay could be related to sequences of Carboniferous metasediments in the Magnitogorsk volcanic arc (Figure 1). Moreover, the seismic recordings display an amplitude attenuation of upper crustal events when crossing from east to west the MUF. Shot record 1 displays a strong decrease in the amplitude of the *Pg* at ≈110-120 km (Figure 10). Shot record 2 shows at this location (at 40 km offset, westward of the shot point) poor signal-to-noise ratio, and a delay of ≈0.2 s in the corresponding *Pg* arrival (Figure 5). These features could be a result of the variation in the physical properties between the former EEC continental crust and the Magnitogorsk volcanic arc.

The weak arrivals visible in all shot gathers at offsets beyond 120 km are correlated with apparent velocities higher than 6 km/s and can be associated with a *PiiP* phase reflected at a midcrustal level. The *PiiP* can be followed as an approximately linear event at 50-100 km offset located at 0.5 s reduced travel time in shot gathers 2 (Figure 5) and 3 (Figure 10). In shot gathers 1 and 4 (Figures 4 and 10) *PiiP* at this offset range (50-100 km) is obscured by the coda of the *Pg* arrival.

Starting at 100 km offset and 3 s reduced travel time, there is a relevant increase in the amplitude of the traces in shot gather 2 (*LC* in Figure 5) for the frequencies above 4 Hz. This event probably corresponds to reflections from the top of the lower crust of the terranes east of the MUF. A high-amplitude event that precedes the *PmP* in shot point 3 between 120 and 170 km offset (*LC* in Figure 4 and phase *PcsP* in Figure 10) is modeled as a reflection of an interface beneath the former discontinuity extending up to 250 km offset and -1 s (Figure 10). These seismic phases suggest the existence of a dipping structure within the lower crust beneath the Magnitogorsk Volcanic arc (Plate 1) where the velocity increases up to values of 6.8-7.0 km/s.

The *PmP* is a prominent event visible beyond 100 km offset in the vertical component record sections and after low pass filtering is imaged in all the shot gathers. For example, in shot record 1 the *PmP* is traced between 100 and 200 km at reduced times of 6 s and 2 s, respectively. This contrasts with shot record 4 which at 120 km offset can be identified at 3 s (Figure 10). The comparison between both shot records implies differences of at least 2 s in the reduced travel time, suggesting lateral differences in Moho depths. Forward modeling of travel times and amplitudes of shot gathers 1 and 4 (Figure 10) indicate that *PmP* is generated by a change in the average velocities from 7.2 ± 0.2 km/s (characteristic of the lower crust) to a mantle velocity of 8.0 ± 0.2 km/s at depths of 50-56 km. The *PmP* phase identified in shot record 1 controls the western part of the root, and its eastern limit is constrained by the fitting of the Moho reflections observed on shot gather 4 (Plate 1). The shape of the crust mantle boundary is controlled by shot point 1 from 35 km up to a distance of 160 km from the western edge

**Figure 10.** (opposite) Vertical component record sections for shot records (a) 1, (b) 4, (c) 2, and (d) 3 (see location in Figure 1) reduced using a 6.0 km/s velocity. The travel time branches predicted by the *P* wave velocity model (Plate 1) are drawn as white lines. This illustrates the agreement of the observed phases and the model predictions. The theoretical travel times were estimated using *Zelt and Smith [1992]*. The phases are *Pg* arrival refracted along the basement, *PiiP* reflection within the middle crust, *PcsP* and *PceP* refer to reflections from the CS and CE interfaces within the lower crust in the model of Plate 1, *PmP* reflection at the crust mantle boundary (Moho). The synthetics generated by the ray tracing scheme of *Zelt and Smith [1992]* showing the amplitude behavior with offset are also displayed for each shot gather.

of the profile (location of the source point 1) ≈15 km east of the MUF. The shape of the root zone beneath the Magnitogorsk volcanic arc is further constrained by the high-amplitude *PmP* observed between 125 and 225 km offsets in shot gather 3. Shot record 2 shows a *PmP* phase characterized by high amplitude onsets that start at 100 km offset and extend beyond 200 km to the east. The *PmP* in shot records 2 and 3 had not been identified in the preliminary interpretatation *[Carbonell et al., 1996]*. Additionally, in all of the vertical component record sections the *PmP* energy reaches a maximum between 125 and 170 km offset (Figure 10). The *PmP* amplitude behavior is well predicted by the forward modeling and the Moho is well constrained from 40 to 280 km in the final model (Plate 1). *PmP* arrivals in shot records 2 and 3 interfere with, and are obscured by, the diffusive long reflectivity train coming from the lower crustal events. In these shot records the lower crust east of the MUF is characterized by a high-frequency, thick reflective band, in contrast with the low-frequency Moho reflected energy in the EEC imaged in shot record 1. These features are indicative of a distinctive structural change beneath the Magnitogorsk volcanic arc implying a significantly different lower crust and Moho beneath the EEC and the Siberian Terranes.

*Pn* arrivals are visible in shot record 4 beyond 300 km offset (Figure 10) and are characterized by high frequencies (6-15 Hz) as they almost disappear when the data are high cut filtered at 6 Hz (Figure 3). The *PmP* and *Pn* constrain a Moho depth that varies from 42-45 at the edges of the profile to 53 ± 3 km beneath the central part, and no indications of marked steps affecting the Moho are observed. Uncertainty estimates of the derived parameters of the model can be made as described by *Zelt and Smith [1992]* and are ≤0.1 km/s for the velocities. The errors in depth of the Moho derived from our data are ≤ 3 km. A 5-km change in the Moho depth would produce *PmP* arrivals which differ in ≈0.5 s from the picked travel times. Further constraints on the depth of the Moho have been discussed elsewhere *[Carbonell et al., 1998]*. Finally, the long wave train that characterizes the *PmP* arrival in shot record 1 at 125-225 km offset and in shot record 3 between 175 and 225 km offset suggests some degree of complexity of the sub-Moho structure beneath the Magnitogorsk volcanic arc.

### 4.2. *S* Wave Data

The record sections of N-S and E-W horizontal components along the main transect after processing show a significant number of *S* wave arrivals that, in general, correspond to those in the vertical components shot records. The comparison between the vertical and the horizontal components of shot records 2 and 3 illustrates that the upper crustal *S* wave reflectivity is higher than the *P* wave reflectivity. The travel times of the *SmS* arrivals for shot records 1 and 4 are not predicted by a simple *S* wave velocity model derived from the $V_p$ model using a conventional Poisson's ratio of 0.25. Moreover, the N-S and E-W components display in some cases prominent differences which vary from shot to shot. Analogous *SmS* phases in the N-S and E-W sections are imaged at different travel times (Figures 8 and 9).

The *Sg* is a prominent high-frequency *S* wave arrival in both the N-S and E-W records sections (Figures 6, 7, 8, and 9). Variations in the travel times of the *Sg* phase correlate with changes in surface geology (Figure 8). A shear wave reflected within the upper crust (labeled *SiiS*) can be identified as a high-amplitude arrival at 40-100 km offset in the N-S component of shot point 1, for frequencies up to 4.5 Hz (Figure 6). The N-S component for shot point 2 also displays a prominent *SiiS* arrival for offsets between 60-125 km range (Figure 8).

Bursts of *S* wave energy coming from the lower crust are marked by an amplitude increase and onsets of reflectivity. For example, a lower crustal arrival is imaged by shot point 3 at 150-220 km offset and -2 s in the N-S record section (Figure 7). It can also be seen on E-W section (*SceS* on Figures 11d and 12 d and *LC* on Figures 7c and d). In the N-S component of shot record 2 the lower crust shows an abrupt increase in reflectivity at 125 km offset and 4 s that can be followed up to 200 km, similar to the vertical component record section (Figure 4). The *ScsS* and the *SceS* lower crustal arrivals are much weaker and more difficult to identify. Nevertheless, shot gather 3 displays a high-amplitude event that matches in travel time the *ScsS* for the offset range betweem 100 and 175 km, and shot record 2 displays an arcuate event over offsets 125 and 175 km, which matches the travel times for the *SceS* phase (Figures 11 and 12).

The *SmS* phase is the most prominent arrival in all the horizontal component record sections, and is visible at shorter offsets than the *PmP*. It is also a low-frequency event with a 1.-1.5 s duration, with a well-resolved starting time; for example, in the N-S and E-W horizontal components of shot record 3 between 100 and 220 km offset (Figures 7, 11, and 12) and in both components of shot records 2 and 4 between 100-230 and 100-330 km offset, respectively (Figures 9, 11, and 12). At 200-250 km offset, there is approximately a 0.5-1 s time difference between the *SmS* arrival for the N-S and E-W horizontal components in shot records 2 and 4 (Figures 8 and 9). The travel time differences in the same S phases observed in the N-S and E-W record sections (Figures 8 and 9) indicated the need for two distinct *S* wave velocity models, $V_s^{NS}$ and $V_s^{EW}$.

The vertical component record sections of shot points 1 and 3 display relatively long *PmP* arrivals, and similar features are distinguished in the horizontal components for shot point 1, which probably denotes a complex sub-Moho structure. Additionally, the N-S component of shot point 3 displays a prominent high-amplitude onset of arrivals beyond 175 km offset after 4 s which also favor a complex upper mantle beneath the Magnitogorsk volcanic arc (Figure 11).

## 5. Discussion

The interpretation of the previously described major seismic events suggests a new and better constrained *P* and *S* wave average velocity models consisting of upper, middle, lower crust and upper mantle (Plate 1). The forward modeling analysis of the wide-angle/refraction data resolves a large scale velocity model in the sense that these are mean

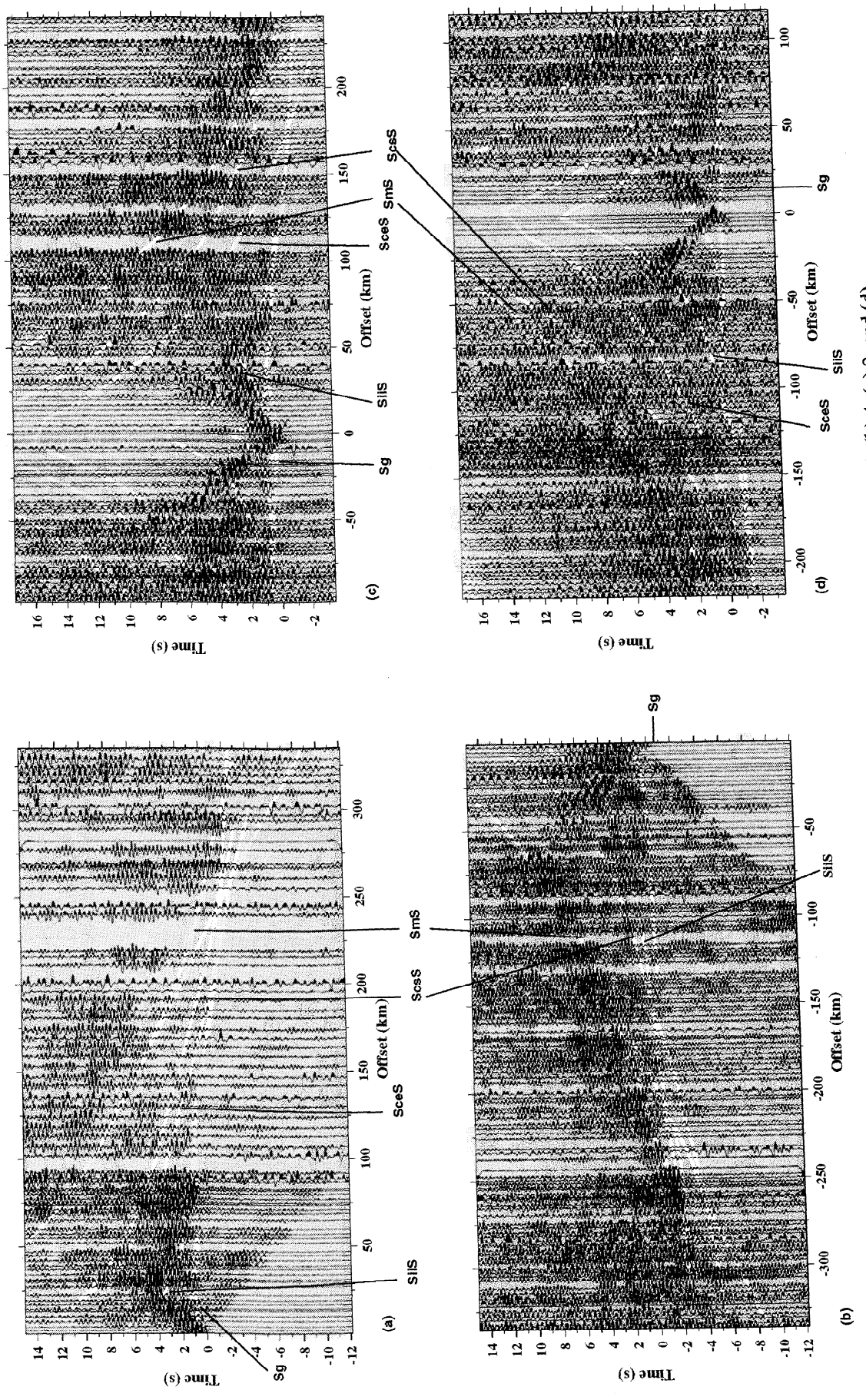


**Figure 11.** N-S oriented horizontal component record sections for shot records (a) 1, (b) 4, (c) 2, and (d) 3 (see location in Figure 1) reduced for a 3.46 km/s velocity. The travel time branches predicted by the final $V_s^{NS}$ velocity model (Plate 1b) are drawn as white lines. This illustrates the agreement of the actual phases and the model predictions. The *S* phases are analogous to the *P* arrivals described in Figure 10.

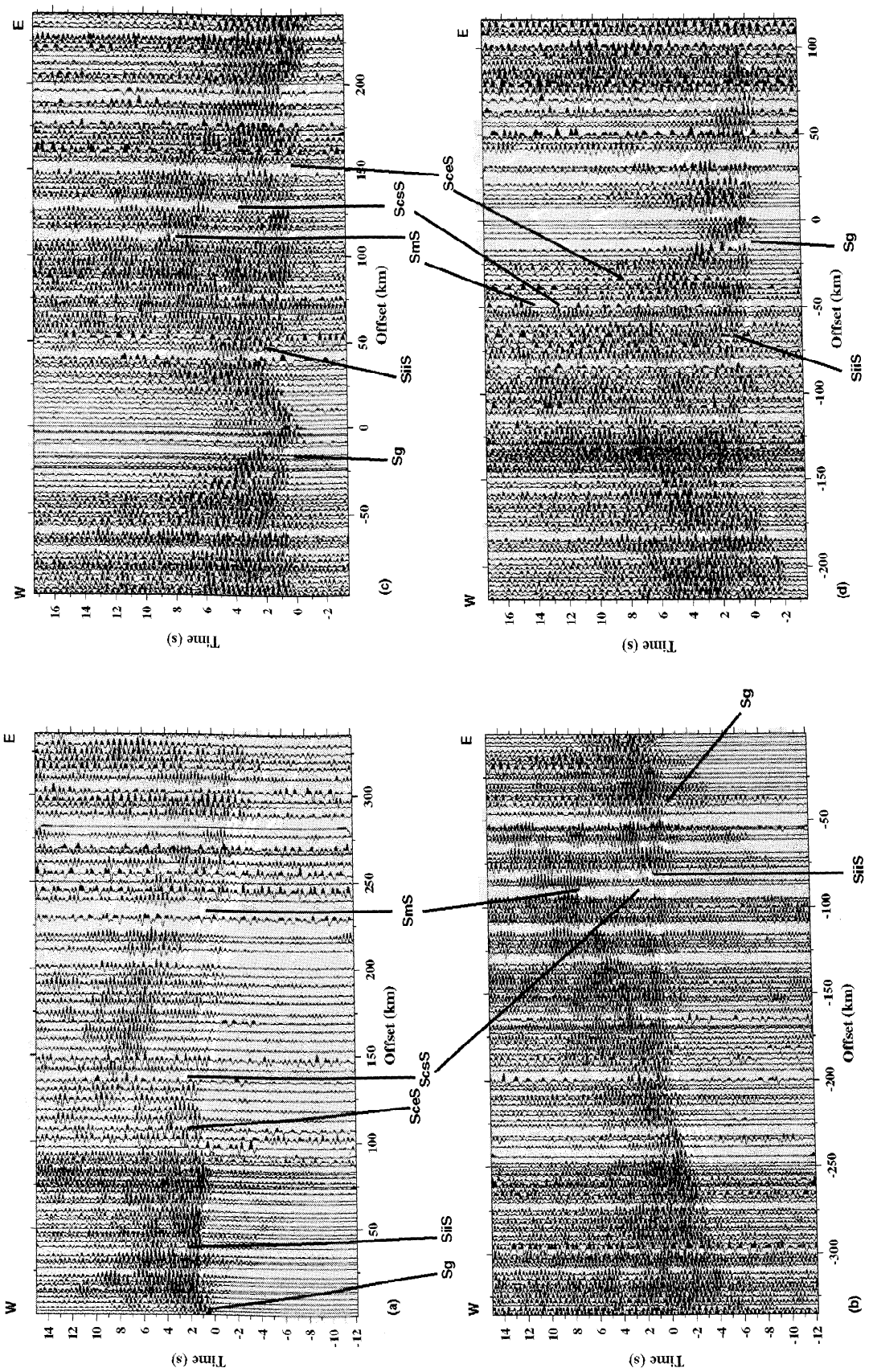


**Figure 12.** E-W oriented horizontal component record sections for shot records (a) 1, (b) 4, (c) 2, and (d) 3 (see location in Figure 1) reduced for a 3.46 km/s velocity. The travel time branches predicted by the final $V_s^{EW}$ velocity model (Plate 1c) are drawn as white lines. The phases correspond to those indicated in Figures 10 and 11.

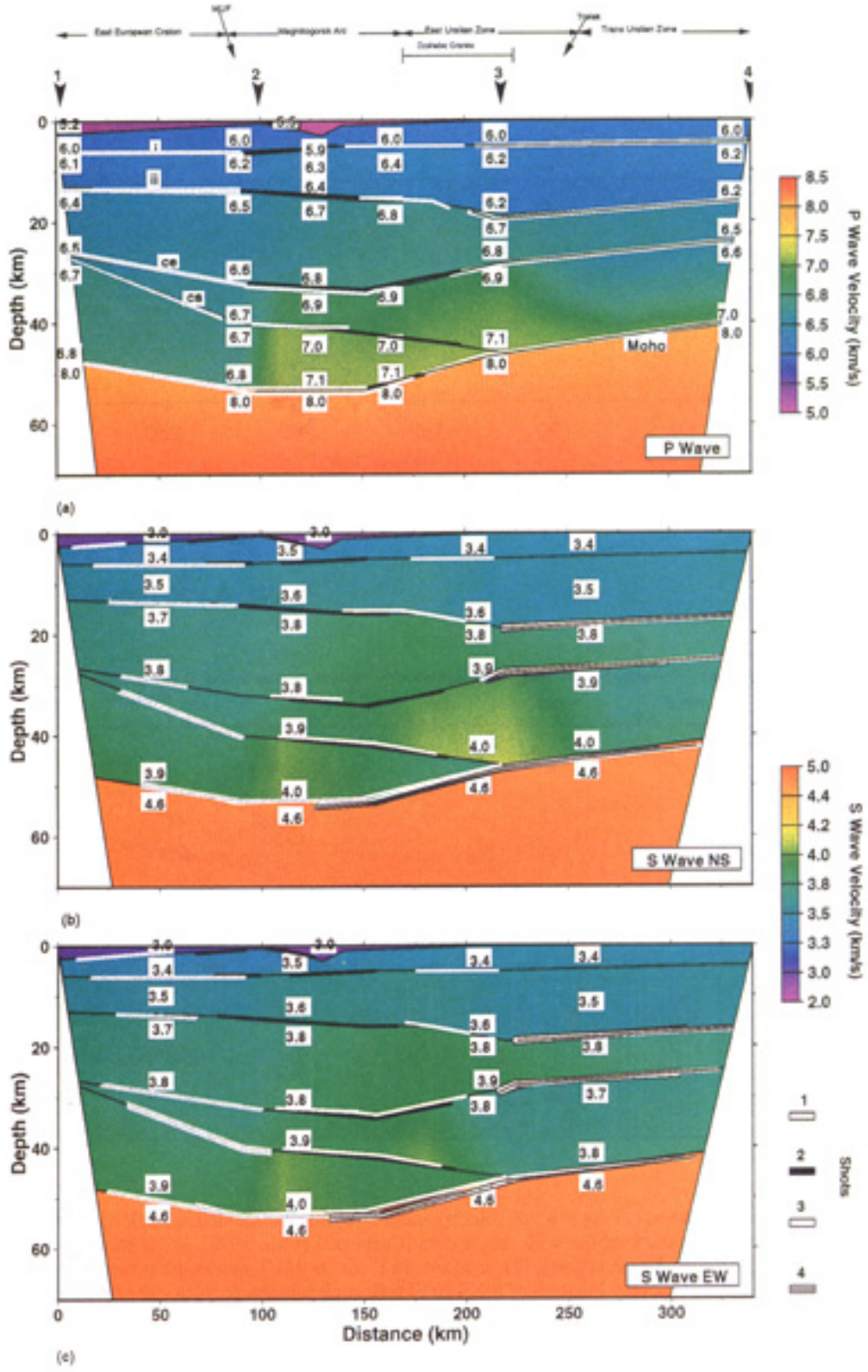


**Plate 1.** Comparison between (a) the *P* wave velocity model, (b) normal incidence stack of the explosion CDP data set, and (c) the stack of the wide-angle data *[Carbonell et al., 1998]*. Note that the reflective Moho weakens beneath the Magnitogorsk volcanic arc. In Plate 2b, MUF marks the position of the main Uralian Fault, and KRS marks the location of the Kartali reflection sequence. Notice the smooth shape of the Moho in the velocity model and in the wide-angle stack.

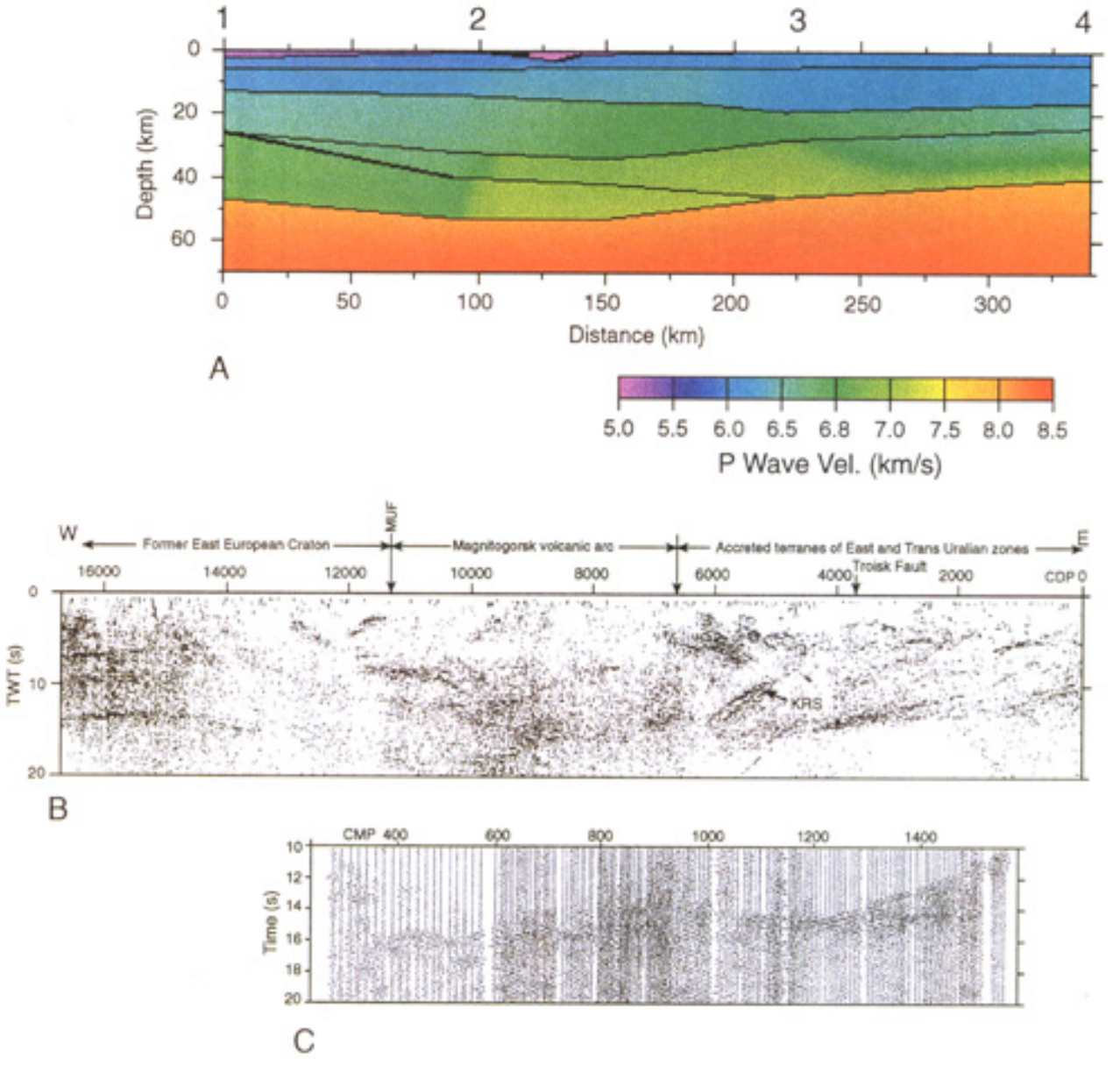


**Plate 2.** Comparison between (a) the *P* wave velocity model, (b) normal incidence stack of the explosion CDP data set, and (c) the stack of the wide-angle data [Carbonell et al., 1998]. Note that the reflective Moho weakens beneath the Magnitogorsk volcanic arc. In Plate 2b, MUF marks the position of the main Uralian Fault, and KRS marks the location of the Kartali reflection sequence. Notice the smooth shape of the Moho in the velocity model and in the wide-angle stack.

velocities averaged along the ray path. The theoretical travel time branches generated by the velocity models are in good agreement within 0.1 s with the observed correlations for all the record sections (Figures 10, 11, and 12).

### 5.1. Seismic Signatures of Crustal Structure and Evolution

The seismic model (Plate 1) features strong lateral variations in shallow velocities in the western end of the transect (between 5.0 and 6.0 km/s), which correlates with the changes in the nature of different tectonic units (the transition from deformed to undeformed Precambrian rocks in pre-Uralide times). This lateral variation of the velocities is derived from the first arrivals at near offsets. Rocks of velocities of 6 km/s crop out in the east Uralian terranes. At depths of 5-7 km the velocities increase up to 6.2-6.3 km/s. The midcrust, from 10 to 30 km depth on average, is characterized by velocities of ≈6.6 km/s. The lower crust, from 30-35 km down to the Moho, has velocities ranging from 6.8 to 7.4 km/s. Poupinet et al., [1997] report a similar velocity-depth function for the middle Urals including a relatively high-velocity lower crust with values ranging from 6.8 to 7.0 km/s. The highest amplitudes for the *PmP* of shot records 1 and 4 are centered between 140 and 170 km offset (Figure 10). The lateral extent (30 km broad area) of this amplitude versus offset (AVO) is indicative of a critical distance for the Moho reflection for these shot records centered at 150 km. Thus, for physically reasonable average velocities for the crust (6.6-6.8 km/s) and mantle (8.0-8.2 km/s), critical distances of 150-170 km imply crustal thicknesses within the range 50-56 km *[Carbonell et al., 1998]*. After low pass filtering high amplitudes are observed in shot records 2 and 3 at similar offsets of 140-170 km (Figures 4, 5, and 11), which support these thickness estimates for the root beneath the southern Urals. Both the vertical and horizontal component record sections suggest structural complexity in the root zone. Thus the root zone is characterized by large lateral variations (velocity and topography of Moho).

A relative increase in the average velocities throughout the crust characterizes the central part of the profile, Magnitogorsk volcanic arc, probably revealing an increase in the metamorphic grade of the rocks in agreement with the surface geologic observations. The reflectivity within the lower crust (see shot point 2 in Figure 5) is limited to the frequency band of 6-15 Hz, suggesting the existence of localized lamination that consists of layers with a dominant thickness ranging between 100-300 m (using $\lambda/4$ criteria *[Fuchs, 1968]*). Localized lamination would also account for the local amplitude anomalies of the lower crustal phases. Crustal lamella or boudinage structures have also been suggested by *Thouvenot et al., [1995]*.

Shot gathers 2 and 3 best document the lower crustal phases *PceP*, *PcsP*, *SceS*, *ScsS*. The vertical component of shot point 1 displays two very close events over 75 and 175 km offset, which are reproduced by the $CS$ and $CE$ interfaces of the final model (Plate 1). The lateral continuity of the phases reflected from the lower crust is indicative of a well-defined velocity change, suggesting a significant change in physical properties at this level within the crust. The $CS$ interface (Plate 1) can be considered as the top of the Precambrian EEC lower crust, while $CE$ can be interpreted as reworked lower crust that resulted from the postorogenic evolution. The layering suggested from the seismic pattern at 100-200 km offset in shot point 2 (Figure 5) supports a complex internal tectonic fabric within the lower crust. A comparison of our velocity model with the normal incidence image (Plate 2) also supports a structurally complex lower crust. The normal incidence explosion data show diffuse reflectivity beneath the Magnitogorsk volcanic arc *[Knapp et al., 1996; Steer et al., 1998]*.

The large trace spacing prevents the spatial resolution of the small scale velocity distribution (e.g., the internal structure of the Moho). However, the heterogeneity of the waveforms of the *PmP* phase (lack of correlation from trace to trace for high frequencies) favors a laterally heterogeneous structure, consisting of lenses, or lamella, probably smaller that 0.25 of a Fresnel radius (the Fresnel radius is of ≈3 km for a 10 Hz signal, 12 s and average velocity of 6.8 km/s). The length and complexity of the *PmP* arrival and the sub-Moho reflectivity (Figures 10, 11, and 12) are probably related to features located at sub-Moho depths. This high-velocity lamella that seem to characterize the lower crust and Moho coupled with the complex upper mantle structure might be a picture of the early stages of crust-mantle interaction mechanisms (equilibration processes). The smooth shape of the Moho beneath the root zone in the southern Urals reflects the ongoing equilibration of the composite Paleozoic collisional Moho to a continental Moho. This post-Triassic feature is probably related to metamorphic phase transitions developed after the collision. However, the smooth shape of the Moho across the southern Urals contrasts with the image obtained north of Ekaterinburg by *Thouvenot et al., [1995]* where an abrupt step in the Moho was interpreted 30-40 km east of the MUF.

The lack of well-defined events in the lower crust specially for the Moho obtained from the normal incidence CMP data set *[Knapp et al., 1996]* contrasts with the image obtained by the wide-angle seismic reflection /refraction data (Plate 2). The lack of Moho in the CMP profile beneath the root zone can probably be explained by the different frequency content of the Moho signals. The CMP data were acquired by conventional oil exploration instrumentation, in particular high-frequency geophones (10-12 Hz) while the wide-angle data were acquired using low frequency sensors (1 Hz). The Moho is imaged when the data are high cut filtered at 6 Hz or even at 4 Hz (Figures 4 and 5). These frequency ranges were not recorded by the CMP data acquisition experiment. The frequency content of the *PmP* phase suggests that the Moho can be considered as a 3-4 km thick layered structure (with an average layer thickness of 0.5-1 km) where the average velocity increases with depth.

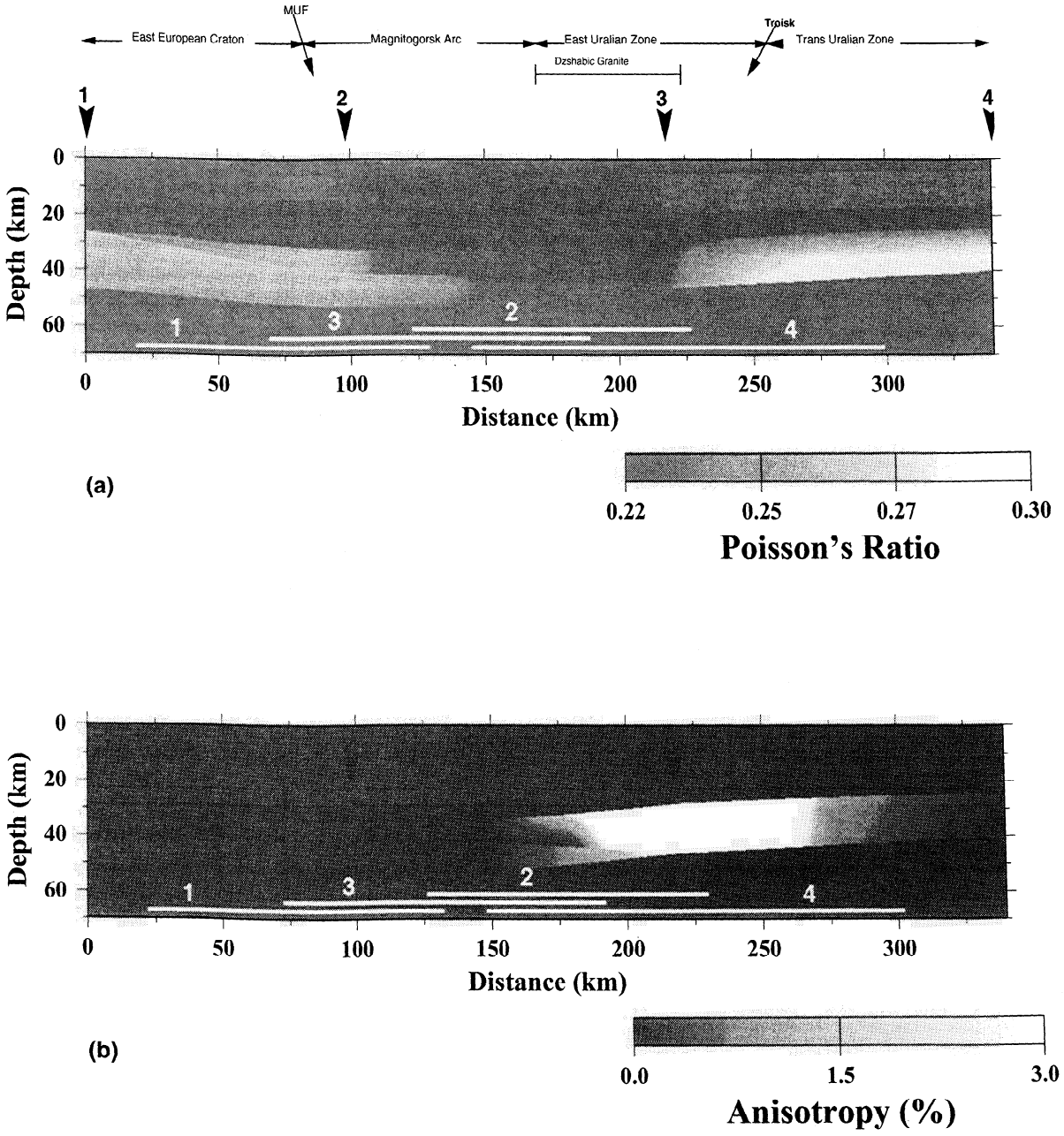


**Figure 13.** (a) Map of the distribution of Poisson's ratios within the crust across the URSEIS'95 transect estimated from equation (1). The most significant tectonic features are outlined above the model. MUF and Troisk denote the surface location of the main Uralian and Troisk faults. (b) Map of the distribution of percent anisotropy within the crust estimated using equation (2). The Kartali reflection sequence (KRS in Plate 2c), a major reflection imaged by the CMP data *[Knapp et al., 1996; Steer et al., 1998]* is located between 20 and 45 km depth range within the range of maximum anisotropy. The anisotropy and the Poisson's ratio beneath the Moho cannot be constrained or resolved because of the lack of data. The *S* wave subsurface coverage for the Moho of the different shot gathers is indicated by white lines in both Figures 13a and 13b; the number above the lines indicates the shot record.

### 5.2. Constraining Heterogeneities and Anisotropic Features: Contribution of *S* Waves

Petrological inferences drawn from *P* wave velocities are strongly nonunique because of the broad range of rock types characterized by the same velocity values. Additional constrains provided by Poisson's ratio estimates can reduce this uncertainty *[Holbrook et al., 1987, 1988, 1992]*. The *S* wave velocity model derived from the *P* wave using a $\sigma$ of 0.25 was not able to predict the travel times for the *SmS* arrivals especially for shot points 1 and 4. In the recordings of these shots the *SmS* is delayed with respect to the *SmS* predicted by the 0.25 model. However, the other crustal *S* phases are predicted correctly by the 0.25 model. The *SmS* phases of shot records 1 and 4 required smaller $V_s$ velocity values for the lower crust (Plate 1) at both sides of the root zone. The

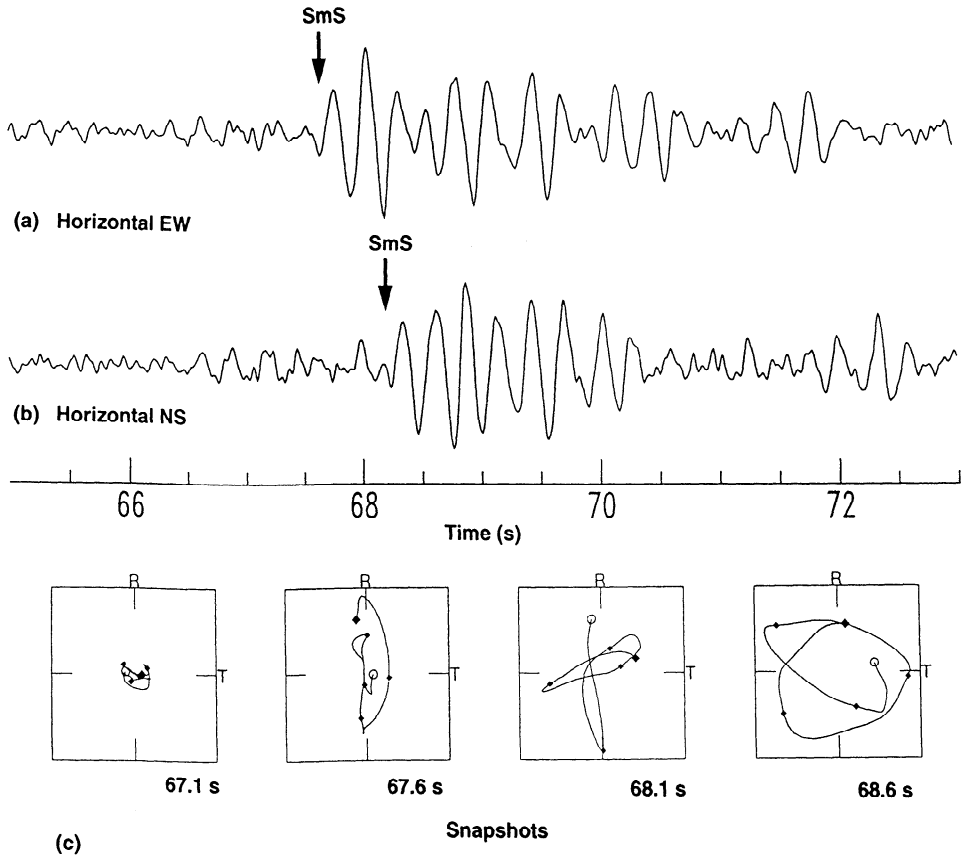


**Figure 14.** Horizontal component seismograms for the (a) E-W and (b) N-S component for shot point 4 at 220 km offset. The *SmS* marks the *S* wave reflected from the Moho. Note the delay of ≈0.5 s between the *SmS* arrivals. (c) Snapshots of the particle motion derived from the horizontal components seismograms. Snapshot at time 67.6 s illustrates that the particle is only moving in the radial direction, while snapshot at time 68.1 s shows a movement in the radial followed by a movement in the transverse direction.

large-scale features of our Poisson's ratio diagram (Figure 13) are well resolved and probably physically meaningful. The upper crust along the profile is characterized by intermediate values of the Poisson's ratio (0.25), which are consistent with rocks of felsic compositions. Poisson's ratio values above 0.25 are estimated for the lower crust at both sides of the root zone, while the central root zone remains close to 0.25. Beneath the EEC, $V_p$ of 6.8-7.0 km/s and $\sigma$ of 0.26-0.28 are consistent with granulite facies rocks with a mafic component *[Rudnick and Fountain, 1995]*. Slightly higher $V_p$ velocities are determined for the lower crust east of the MUF, favoring an increase in the mafic component (perhaps a mixture of intermediate to mafic granulites).

A root zone consisting of intermediate granulites can account for the $\sigma$ values (close to 0.25) and the relatively high $V_p$ determined for the lower crust beneath the Magnitogorsk volcanic arc. An alternative interpretation is that the granulitic lower crust of the root zone has been partially eclogitized, as part of the equilibration mechanisms. This process would decrease the high $\sigma$ values typical of mafic granulites to values approaching 0.25. A crust-mantle transition consisting of an interlayered sequence of peridotite, dunite, eclogite is consistent with the seismic observations (frequency content, $P$ and $S$ wave velocities, Poisson's ratio).

The velocity model $V_s^{NS}$ was not able to predict the *SmS* travel times of the E-W oriented horizontal component record sections (specially the *SmS* of shot record 2 and 4). The other upper and lower crustal phases are correctly predicted by the same $V_s$ velocity model. The comparison between $V_s^{NS}$ and $V_s^{EW}$ shows differences in the velocity of polarized $S$ waves. Also other explanations can account for the time differences between *SmS* in the N-S and E-W recordings. The time delay could be a result of three-dimensional structure affecting the ray path or that one of the components is affected by S to P conversions. Nevertheless, the particle motion diagrams derived from individual *SmS* arrivals identified in the N-S and E-W components provide further evidence (Figure 14) for this localized anisotropy. The Kartali reflection sequence (KRS) (Plate 2b) identified in the CMP data *[Knapp et al., 1996]* is located within this extended anomaly (at 175-275 km from the origin of the model, Figure 13 and Plate 2), characterized by relative high anisotropy values (2-3%). Tectonic fabrics are a reasonable candidate to account for the reflectivity in the CMP image and the anisotropy mapped by the wide-angle

data. This feature is located beneath the Dzhabic Granite and could be related to its emplacement.

## 6. Conclusions

A basic feature established from this study is that the wide-angle reflectivity beneath the southern Urals has a strong frequency dependence. The lower crust is characterized by a frequency band between 6 and15 Hz, and the *PmP* is characterized by low frequencies up to 6 Hz. The wide-angle seismic reflection/refraction data provide the most reliable evidence for the depth extent of the crustal root beneath the central part of the southern Urals. The crustal thickness increases from 43 to 45 km at the margins of the transect up to 53-56 km beneath the central part of the profile. Well defined seismic phases are the basis for estimating average P- and *S* wave velocity models for the crust: an upper layer of 5.0-6.0 km/s which correlates with the surface geology; at depths of 5-7 km the velocities increase up to 6.2-6.3 km/s; from 10 to 30 km depth on average the crust is characterized by velocities of ≈6.6 km/s and, finally, the lower crust, from 30-35 km down to the Moho, has velocities ranging from 6.8 to 7.4 km/s. *P* wave velocities of 8.0-8.2 km/s and *S* wave velocities of 4.5-4.7 km/s are characteristic of the upper mantle. A relative increase in the average *P* and *S* wave velocities characterizes the central part of the profile (Magnitogorsk volcanic arc) and is possibly indicative of an increase in the metamorphic grade in the crust. The EEC features Poisson's ratio values ¡ 0.25 which contrasts with the crust of the accreted terranes to the east which features normal values ≈0.25. At each side of the root, two localized maxima delineate the Moho. The lateral changes in the reflectivity pattern indicate differences in the nature of the lower crust at both sides of the MUF. Although the trace spacing is too large for a high-resolution image of the small-scale velocity variations (internal structure of the reflecting horizons), the frequency content suggests a complex lamellae structure for the lower crust and Moho. The high average velocities at lower crustal depths indicate a possible increase in rocks with mafic composition. The thickness increase, the velocity, and the lateral variability of the Moho are evidence for lateral changes in the nature of crust-mantle boundary beneath the southern Urals that may reveal different genetic origins. The constraints determined from the wide-angle data suggest a 3-5 km thick layered Moho consisting of lamellae of 0.5-1 km thickness. This Moho reflects ongoing equilibration of the composite Paleozoic collisional Moho to a continental Moho. This post-Triassic feature is probably indicating metamorphic phase changes which resulted in an interlayered sequences of eclogites and mantle. Eclogite layers within the upper mantle could be responsible for the sub-Moho events.

**Acknowledgments.** We are specially thankful to the field crew for their effort in the acquisition of these data. S. Kruse and T. Brocher provided very helpful comments to a first version of this manuscript. This paper benefited from the careful reviews by J. Ansorge and J. McBride. We would also like to thank D. Brown for his suggestions. This research was carried out in association with the EUROPROBE Uralides Project. Funding for the URSEIS'95 seismic experiment was provided by the Comisi'on Interministerial de Ciencia y Technologíia (CICYT, Spain) grants AMB 95-09987E, UE95-0026; ROSCOMNEDRA (Russia); DEKORP 2000 (German Federal Ministry of Science and Technology research grant 03GT94101 with additional support from the German Science Foundation). The Continental Dynamics Program (N-SF grant EAR-9418251 (USA), and International Association for the Cooperation with Scientist from the Former Soviet Union grant 94-1857.

## References

Aleinikov, A., O. Bellavin, B. Diakonov, and A. Krasnobayeba, Deep crustal structures of the Urals and their connection with the planetary anomalies, in *N.A. Bogdanov and Tesizy, 27 y mezhdunarodn geologichskiy kongress Abstracts, Proc. Int. Geol. Congr.*, 27, 11–15, 1984.

Avtoneyev, S., et al., Deep structure of the Urals from geophysical data, *Int. Geol. Rev.*, *34*, 263–279, 1992.

Berzin, R., O. Oncken, J. Knapp, A. P.-E. T. Hismatulin, N. Yunusov, and A. Lipilin, Orogenic evolution of the Ural Mountains: Results from an integrated seismic experiment, *Science*, *274*, 220–221, 1996.

Brown, D., V. Puchkov, J. Alvarez-Marrón, and A. Pérez-Estaún, The structural architecture of the footwall to the Main Uralinan Fault, southern Urals, *Earth Sci. Rev.*, *40*, 125–147, 1996.

Brown, D., C. Juhlin, J. Alvarez-Marrón, A. Pérez-Estaún, and A. Oslianski, Crustal-scale structure and evolution of an arc-continent collision zone in the southern Urals, *Tectonics*, *16*, 551–562, 1997.

Carbonell, R., A. Pérez-Estaún, J. Gallart, J. Diaz, S. Kashubin, J. Mechie, R. Stadtlander, A. Schulze, J. Knapp, and A. Morozov, Crustal root beneath the Urals: Wide-angle seismic evidence, *Science*, *274*, 222–223, 1996.

Carbonell, R., D. Lecerf, M. Itzin, J. Gallart, and D. Brown, Mapping the Moho beneath the southern Urals with wide-angle reflections, *Geophys. Res. Let.*, *25*, 4229–4232, 1998.

Döring, J., H. Götze, and M. Kaban, Preliminary study of the gravity field of the southern Urals along the URSEIS'95 seismic profile, *Tectonophysics*, *276*, 49–62, 1997.

Druzhinin, V., S. Kashubin, V. Rybalka, and L. Sharmanova, Osobennosti metodiki i rezulfaty glubinnykh seismicheskikh issledovanity na kranourralśkom profile gsz, in *Seismorazvedka pri Poiskakh Mestorozheniy Tsvetnykh Metallov na Urale. Geogicheskiy Fond RSFSR*, edited by V. Antonov, N. Ermakov, N. K. Y. Menśhikov, V. Rybalka, and Z. Sega, pp. 103–119, Fond RSFSR, Moscow, 1981.

Druzhinin, V., S. Kashubin, S. Avtoneev, S. Avtoneyev, and V. Rybalka, New data on deep structure of the southern Urals according to results of investigations on the Troitsk DS profile, *Soviet Geol. and Geophys.*, *29*, 79–82, 1988.

Echtler, H., M. Stiller, F. Steinhoff, C. Krawczyk, A. Suleimanov, V. Spiridonov, J. Knapp, Y. Menshikov, J. Alvarez-Marrón, and N. Yunusov, Preserved collisional crustal structure of the southern Urals revealed by Vibroseis profiling, *Science*, *274*, 224–226, 1996.

Egorkin, A. and A. Mikhaltsev, The results of seismic investigations along geotraverses, in *Superdeep Continental Drilling and the Deep Geophysical Sounding*, edited by K. Fuchs, Y. Kozlovsky, A. Kristsov, and M. Zoback, pp. 111–119, Springer-Verlag, New York, 1990.

Fershtater, G., P. Montero, N. Borodian, E. Pushkarev, V. Smirnov, and F. Bea, Uralian magmatism: An overview, *Tectonophysics*, *276*, 87–102, 1997.

Fuchs, K., On the properties of deep crustal reflectors, *J. Geophys.*, *35*, 133–149, 1968.

Gee, D. and H. Zeyen, *EUROPROBE 1996 - Lithospheric Dynam-*

*ics: Origin and Evolution of Continents*, Uppsala Univ., Uppsala, Sweden, 1997.

Hamilton, W., The Uralides and the motion of the Russian and Siberian platforms, *Geol. Soc. Am. Bull.*, *81*, 2553–2576, 1970.

Holbrook, W., D. Gajewski, and C. Prodehl, Shear wavevelocity and Poisson's ratio structure of the upper lithosphere in Southwest Germany, *Geophys. Res. Lett.*, *14*, 231–234, 1987.

Holbrook, W., D. Gajewski, A. Krammer, and C. Prodehl, An interpretation of Wide-Angle compressional and shear wave data in Southwest Germany: Poisson's ratio and petrological implications, *J. Geophys. Res.*, *93*, 12081–12106, 1988.

Holbrook, W., W. Mooney, and N. Christensen, The seismic velocity structure of the deep continental crust, in *Continental Lower Crust*, edited by D. Fountain, R. Arculus, and R. Kay, pp. 1–44, Elsevier Sci., New York, 1992.

Ivanov, K. and S. Ivanov, Structural correlation between main volcanic zones of the Urals-Tagil-Magnetogorsk, *Dolk. Akad. Nauk. SSSR*, *285*, 177–180, 1991.

Ivanov, S. and A. Rusin, Model for the evolution of the linear fold belt in the continents: Example of the Urals, *Tectonophysics*, *127*, 383–397, 1986.

Ivanov, S., A. Perfiliev, A. Efimov, G. Smirnov, V. Necheukhin, and G. Fershtater, Fundamental features in the structure and evolution of the Urals, *Am. J. Sci.*, *275*, 107–130, 1975.

Juhlin, C., S. Kashubin, J.H. Knapp, V. Makovsky, and T. Ryberg, Project. conducts seismic reflection profiling in the Ural Mountains, *Eos Trans. AGU*, 193, 197–199, 1995.

Juhlin, C., M. Bliznetsov, L. Pevzner, T. Hismatulin, A. Rybalka, and A. A. Glushkov, Seismic imaging of reflectors in the SG4 borehole, Middle Urals, Russia, *Tectonophysics*, pp. 1–18, 1997.

Khain, V., *Geology of the USSR*, Schweizerbartsche Borntanger, Stuttgart, 1985.

Knapp, J., D. Steer, L. Brown, R. Berzin, A. Suleimanov, M. Stiller, E. Lüshen, D. Brown, R. Bulgakov, S. Kashubin, and A. Rybalka, Lithosphere-Scalc seismic image of the southern Urals from explosion-source reflection profiling, *Science*, *274*, 226–228, 1996.

Kruse, S. and M. McNutt, Compensation of Paleozoic orogens: A comparison of the Urals to the Appalachians, *Tectonophysics*, *154*, 1–17, 1988.

Lucas, S., A. Green, Z. Hajnal, D. White, J. Lewry, K. Ashton, W. Weber, and R. Clowes, Deep seismic profile across a Proterozoic collision zone. Surprises at depth, *Nature*, *363*, 390–392, 1993.

Matte, P. and A. Hirn, Seismic signature and tectonic cross section of the variscan crust in western France, *Tectonics*, *7*, 141–155, 1988.

Matthews, D. H. and M. Cheadle, Deep reflections from the Caledonides and Variscides west of Britain and comparison with the Himalayas, in *Reflection Seismology: A Global Perspective*, *Geodyn. Ser.*, vol. 13 edited by M. Barazangui and L. Brown, pp. 3–19, AGU, Washington, D.C., 1986.

McBride, J. and K. Nelson, Deep seismic reflection constraints on Paleozoic crustal structure and definition of the Moho in the buried Southern Appalachian orogen, in *Continental Lithosphere: Deep seismic reflections*, *Geodyn. Ser.*, vol 22, edited by R. Meissner, L. Brown, H. Dürbaum, W. Franke, K. Fuchs, and F. Seifert, pp. 9–20, AGU, Washington, D.C., 1991.

Meissner, R. and T. Wever, Nature and development of the crust according to deep reflection from the German Variscides, in *Reflection Seismology: a Global Perspective*, *Geodyn. Ser.*, vol. 13, edited by M. Barazangui and L. Brown, pp. 31–42, AGU, Washington, D.C., 1986.

Pérez-Estaún, A., J. Alvarez-Marrón, D. Brown, V. Puchkov, Y. Gorozhanina, and V. Baryshev, Along-strike structural variations in the foreland thrust and fold belt of the Southern Ural, *Tectonophysics*, *276*, 265–280, 1997.

Poupinet, G., F. Thouvenot, E. Zolotov, P. Matte, and A. E. V. Rackitov, Teleseismic tomography across the middle Urals: Lithospheric trace of an ancient continental collision, *Tectonophysics*, *276*, 19–34, 1997.

Puchkov, V., Structure and geodynamics of the Uralianorogen, in *Orogeny Through Time*, edited by J. Burg and M. Ford, Geol. Soc. Spec. Public., *121*, 201–236, 1997.

Rudnick, R. and D. Fountain, Nature and composition of the continental crust: A lower crustal perspective, *Rev. Geophys.*, *33*, 267–309, 1995.

Ryzhiy, B. P., V. Druzhinin, F. Yunusov, and I. Ananyin, Deep structure of the Urals region and its seismicity, *Phys. Earth Planet. Int.*, *75*, 185–191, 1992.

Seravkin, I., A. Kosarev, and D. Salikhov, Volcanism of the southern Urals, 195 pp. Nauka, Moscow, 1992.

Seward, D., A. Pérez-Estaún, and V. Puchkov, Preliminary fission-track results from the Southern Urals-Sterlitamak to Magnitogrosk, *Tectonophysics*, *276*, 281–290, 1997.

Sheriff, R. and L. Geldart, *Exploration Seismology*, Cambridge Univ. Press, New York, 1982.

Sokolov, V., The structure of the Earth's crust in the Urals, *Geotectonics*, *5*, 3–19, 1992.

Steer, D., J. Knapp, L. Brown, H. Echtler, D. Brown, and R. Berzin, Deep Structure of the continental lithosphere in an unextended orogen: Explosive source seismic reflection profile across the Urals (URSEIS 1995), *Tectonics*, *17*, 143–157, 1998.

Thouvenot, F., S. Kashubin, G. Poupinet, V. M. ad T.V. Kashubina, P. Matte, and L. Jenatton, The roots of the Urals: Evidence from wide-angle reflection seismics, *Tectonophysics*, *250*, 1–13, 1995.

Veis-Ksenofontova, Z. and V. Popov, Kvoprousu o seismic heskoei kcharakteristice Urala, *Tr. Seismol. Inst. AN SSSR,*, *104*, 1–12, 1940.

Yilmaz, O., *Seismic Data Processing*, *Investigations in Geophys.*, vol 2, Soc. Explor. Geophys., Tulsa, Okla., 1987.

Zelt, C. and R. Smith, Seismic traveltime inversion for 2-D crustal velocity structure, *Geophys. J. Int.*, *108*, 16–36, 1992.

Zonenshain, L., V. Korinevsky, V. Kazmin, D. Pechersky, V. Khain, and V. Mateveenkov, Plate tectonic model of the south Urals development, *Tetonophysics*, *109*, 95–135, 1984.

Zonenshain, L., M. Kuzmin, and L. Natapov, Uralian Foldbelt, in *Geology of the USSR: A Plate-Tectonic Synthesis*, *Geodynamic Series*, vol. 21, edited by B. M. Page, vol. 21 of pp. 27–54, AGU, Washington, D.C., 1990.

R. Carbonell, J. Diaz, J. Gallart and A. Pérez-Estaún, Dept. of Geophysics, Inst. de Ciències de la Terra "Jaume Almera" Consejo Superior de Investigaciones Científicas, Lluí Solé Sabarís s/n, Barcelona, Spain. (rcarbo@ija.csic.es; jdiaz@ija.csic.es; jgallart@ija.csic.es; andres@ija.csic.es)

S. Kashubin, Bazhenov Geophysical Expedition, Scheelite, 624051 Russia. (uricc@dialup.mplik.ru)

J. Mechie, GFZ, Potsdam, D-14473 Potsdam, Germany. (jimmy@gfz-potsdam.de)

F. Wenzel, Geophysical Institute, Karlsruhe University, Hertzstrasse 16, 76187 Karlsruhe, Germany. (fwenzel@gpiwap1.physik.uni-karlsruhe.de)

J. Knapp, INSTOC, Cornell University, 4132 Snee Hall, Ithaca, NY 145853, USA. (jhk8@cornell.edu)

(Received September 30, 1999; revised December 3, 1999; accepted February 14, 2000.)